Throughput Maximization for Backscatter- and Cache-Assisted Wireless Powered UAV Technology

Dinh-Hieu Tran, *Graduate Student Member, IEEE*, Symeon Chatzinotas, *Senior Member, IEEE*, and Björn Ottersten, *Fellow, IEEE*

***Abstract*—This paper investigates a wireless powered unmanned aerial vehicle (UAV) communication network with backscatter and caching technologies. Specifically, we assume a self-energized UAV with a cache memory is deployed as a flying backscatter device (BD), term the UAV-enabled BD (UB), to relay the source's signals to the destination. Whereas the source S can act as a wireless charging station or a base station to supply power or transmit information to the UB using the dynamic time splitting (DTS) method. The UAV utilizes its harvested energy for backscattering (i.e., passive communication) and transmit information (i.e., active communication) to the destination. In this context, we aim to maximize the total throughput by jointly optimizing the DTS ratio and the UB's trajectory with caching capability at the UB. The formulation is troublesome to solve since it is a non-convex problem. To find solutions, we decompose the original problem into two sub-problems, whereas we first optimize the DTS ratio for a given UB's trajectory and the UB's trajectory optimization for a given DTS ratio. By using the KKT conditions, a closed-form expression for the optimal value of the DTS ratio is obtained, greatly reducing the computation time. Moreover, the solution of the second sub-problem can be acquired by adopting the successive convex approximation (SCA) technique. Consequently, an efficient alternating algorithm is proposed by leveraging the block coordinate descent (BCD) method. To show the advantages of the proposed BCD-based algorithm, we also provide the solution of the original problem applying the inner approximation (IA) method. Finally, the intensive numerical results demonstrate that our proposed schemes achieve significant throughput gain in comparison to the benchmark schemes.**

***Index Terms*—Backscatter communication (BackCom), caching, energy harvesting, reflection coefficient control, time allocation, trajectory design, SWIPT, unmanned aerial vehicle (UAV).**

I. Introduction

UNMANNED aerial vehicles (UAVs) have attracted significant attention from both academia and industry due to their flexible deployment, low cost, and high maneuverability [1], [2]. Indeed, UAVs have enabled various applications such as military, agriculture, transportation, search and rescue missions, surveillance and monitoring, telecommunications [1]–[8]. Particularly, if properly designed and deployed, UAVs can provide efficient solutions for wireless communication networks. Specifically, UAVs can be utilized as aerial/flying base stations (BSs) to support terrestrial BSs that are located in fixed locations and cannot be shifted elsewhere. Especially, in a natural disaster where terrestrial BSs are damaged or isolated, portable BSs do exist but they have to be moved using ground vehicles which is problematic when infrastructures for publication transportation systems may be destroyed. Consequently, UAVs can be swiftly deployed to disseminate vital information to people or help them to communicate with authorities as soon as possible [3], [7]. For industrial applications, Google Project Wing and Amazon Prime Air have built and tested drones deliveries that could be used after a disaster (i.e., flood, earthquake) or in extreme weather conditions [9]. They expect to develop an advanced delivery system where drones help to bring medications or foods to people in the areas that conventional vehicles can not reach. Besides, Facebook Halts Aquila and Google Loon projects aim at beaming internet access to people around the world who cannot connect to the Internet by using drones/balloons [10]. Furthermore, AT&T and Qualcomm are planning to adopt UAVs for facilitating large-scale wireless communications in 5G networks [11].

UAVs have been proposed as relays to improve the connectivity of networks [7], [12]–[17]. Especially, in case direct communications links are missing due to shadowing or un-communication devices by the BSs during peak hours. In these cases, UAVs are deployed as relays to help convey information from source to destination. In [12], the authors studied UAVs-assisted self-organized device-to-device (D2D) networks. Specifically, they aimed to maximize the total throughput via jointly optimizing the channel allocation, relay deployment, and relay assignment. Li *et al.* [13] investigated the joint positioning and power control to maximize the sum rate of UAV relay networks, wherein the UAV utilized two-way communications between the BS and a set of users. The works in [14] and [15] investigated the secure transmission in UAV relay networks. Sharma *et al.* in [14] proposed a novel secure 3D UAV relaying for hybrid satellite-terrestrial networks (HSTNs) in the presence of a flying eavesdropper and then they investigate secrecy outage probability and the probability of non-zero secrecy capacity. Sun *et al.* [15] studied secure transmissions of millimeter-wave simultaneous wireless information and power transfer (SWIPT) UAV relay networks with multiple eavesdroppers. In contrast to [12]–[16] that only considered half-duplex (HD), [7] and [17] investigated the rotary-wing UAV-enabled FD Internet-of-Things (IoT) networks.

Manuscript received July 14, 2021; revised December 13, 2021; accepted February 25, 2022. Date of publication March 1, 2022; date of current version May 20, 2022. This work was supported in part by the Luxembourg National Research Fund through Project FNR CORE ProCAST under Grant C17/IS/11691338 and in part by FNR 5G-Sky under Grant C19/IS/13713801. The review of this article was coordinated by Dr. Huiling Zhu. *(Corresponding author: Dinh-Hieu Tran.)*

The authors are with the Interdisciplinary Centre for Security, Reliability and Trust (SnT), University of Luxembourg, 4365 Esch-sur-Alzette, Luxembourg (e-mail: hieu.tran-dinh@uni.lu; symeon.chatzinotas@uni.lu; bjorn.ottersten@uni.lu).

Digital Object Identifier 10.1109/TVT.2022.3155190

Recently, backscatter communication (BackCom) has emerged as a key concern for UAV communication networks [8], [18]–[21] since a typical backscatter circuit's power consumption is usually in the order of μW [22]–[24]. In [8], the authors proposed two novel schemes termed the transmit-backscatter protocol and transmit-backscatter relay protocol corresponding to the presence or absence of a direct link between backscatter user and receiver in UAV-aided BackCom networks. Yang *et al.* [18] considered a UAV-aided BackCom network comprising of backscatter devices (BDs) and carrier emitters (CEs) that are randomly distributed on the ground. They aimed at maximum energy efficiency (EE) by jointly optimizing the BDs' scheduling, the UAV's trajectory, and the CEs' transmit power. Farajzadeh *et al.* [19] proposed a novel UAV data collection in NOMA BackCom networks, where the UAV acted both as a power source and a data collector. The objective was to jointly design several backscatter devices, UAV's altitude, and backscatter coefficient to maximize the total successfully decoded bits while minimizing the UAV's flight time. The same authors in [20] studied the first work that considered UAV as an enabler to improve over-the-air computation (AirComp)'s performance. Hu *et al.* [21] proposed the first work that investigated secure transmissions in UAV-aided BackCom networks.

Although UAV-enabled BD (UB) can significantly reduce power consumption compared to active transmission, i.e., μW versus Watts, the main power consumption of UAV is propulsion energy, i.e., in hundred Watts [4], [5]. Moreover, a restricted onboard battery is one of the inherent limitations of the UAV, which greatly affects the UAV lifetime and performance in practice. To overcome this problem, there are some papers that investigate energy consumption trade-offs or energy-efficient systems [25], [26]. Besides, wireless power transfer (WPT) has emerged as a promising solution to tackle this issue due to its controllability and predictability compared to other ambient source such as wind, vibration, and solar [27], [28]. Thanks to the development of WPT technology that can transfer power to the user at a distance of up to 6.3 km [29]–[31], which can benefit UAV-assisted communications. Particularly, there has been reports on solutions for battery-free drone that can fly forever with wireless power [32], [33]. Specifically, the demo in [33] showed that a heavy drone with peak power consumption up to 450 Watts and was powered completely wirelessly. As a research upsurge, wireless powered UAV is a hot topic that receives considerable attention from researchers [34]–[36]. Yin *et al.* [34] investigated a downlink (DL) cellular network, whereas multiple UAVs were powered by a ground charging station using save-then-transmit scheme. Jayakody *et al.* [35] proposed a new self-energized UAV system, where they considered an EH scheme including WPT, simultaneous wireless information and power transfer (SWIPT), and self-interference from full-duplex (FD) mode. Yan *et al.* [36] studied a UAV-enabled wireless sensor network (WSN) in which the UAV harvested energy from the base station (BS), then it used this harvested energy to serve multiple WSNs to maximize total energy received by all sensors. Despite prominent achievements in UAV-assisted BackCom networks in [8], [18]–[21] and in wireless powered UAV [34]–[36], aforementioned works do not take caching into consideration.

Recent works have shown that some popular files are repeatedly demanded by users, which accounts for a massive portion of data traffic [37], [38]. By storing a part of popular content in the cache of edge nodes, wireless caching is a promising method to reduce traffic load, especially during peak hours. Some recent works such as in [39]–[43] have been recently devoted to cache-assisted UAV communications. Xu *et al.* [39] proposed a novel scheme to overcome the endurance issue at the UAV by utilizing proactive caching. Specifically, they aimed at minimizing the weighted sum of the file caching cost and the retrieval cost by jointly optimizing the UAV communication scheduling, UAV trajectory, and file caching policy. Cheng *et al.* [40] proposed a novel scheme to assure the secure transmission for UAV relay networks with caching capability. The learning-based approaches in cache-enabled UAV communications were investigated in [41]–[43]. Chen *et al.* [41] proposed the first work to analyze the utilization of caching in UAV communications based on conceptor-based echo state networks (ESNs). Different from existing works that focused on finite-time horizon offline trajectory design, Chai *et al.* [42] proposed an online trajectory and resource allocation optimization for cache-enabled UAV wireless communications. Wu *et al.* [43] adopted a convolutional neural network (CNN)-based deep supervised learning scheme for pushing up the decision-making speed in the highly dynamic vehicular networks. In [44], a multi-agent meta reinforcement learning (RL) solution was first applied in designing trajectories for a group of UAVs in dynamic and unpredictable wireless environments.

From the above discussions and the fact that wireless power, caching and BackCom are energy-efficient communication technologies for UAV communication networks, this paper investigates a caching UAV-enabled BackCom network with SWIPT, in which a UAV can store a part of popular contents in its cache. Besides, the UAV is equipped with a energy harvester circuit that can harvest the RF signal from the source and then use this energy for BackCom and active transmission to the destination. In contrast to the above works in [8], [18]–[21] that only consider UAV as a transmitter/receiver, this work considers UAV as an aerial BD which harvests energy from the source's RF signal and then utilizes this energy for backscattering signal to the destination. *To our best knowledge, this is the first work that jointly considers the combination of SWIPT, caching and backscatter in UAV networks.* In summary, our contributions are as follows:

- We propose a novel backscatter- and cache-assisted wireless powered UAV communication network. Specifically, caching and backscatter can reduce the power consumption while source S provides power to the UAV, thus overcoming the sustainability issue in the UAV. In particular, this is the first work that jointly considers UAV, SWIPT, caching, and BackCom, which imposes great challenges in system modeling and problem-solving.
- Because the UB flies from initial to final locations, it cannot hover over the source all the time. Thus, the dynamic time splitting (DTS) ratio and the UB trajectory should be carefully designed to maximize the total system throughput while still satisfying the energy constraint. If τ_n is large, thus more time is allocated for data transmission but less time is used for energy harvesting and vice versa. Consequently, there exists a trade-off for the DTS ratio in each time slot which directly impacts the amount of harvested energy and data rate.
- Motivated by the above considerations, we formulate an optimization problem to maximize the total collected throughput at the destination, subject to constraints on the

limited flying time, UB's maximum speed, UB's trajectory, and DTS ratio in each time slot. The formulation is non-convex problem and challenges to be solved.

- We decompose the problem into two sub-problems, wherein we first optimize the DTS ratio for a given UB's trajectory, followed by the trajectory optimization for a given DTS ratio. Particularly, the closed-form expressions for the DTS ratio is derived which dramatically reduces the computation time. The trajectory optimization sub-problem can be solved by leveraging the successive convex approximation (SCA) technique. Based on the solutions of these sub-problems, we propose two-layer alternating algorithms to solve formulated problems adopting the block coordinate descent (BCD) method.
- To fully investigate the effectiveness of solutions to the original problem, we also provide the solution utilizing the inner approximation (IA) method besides the proposed BCD-based algorithm.
- The effectiveness of the proposed schemes is demonstrated via numerical results, which show significant enhancements concerning the total collected throughput at the destination in comparison to the benchmark schemes. Specifically, the benchmark schemes are designed similar to that of our proposed algorithm but without caching capability or with a fixed DTS ratio or with a fixed trajectory.

The rest of the paper is organized as follows. The system model and problem formulation are given in Section II. The proposed iterative algorithm for solving linear EH model-based UAV-enabled BackCom is presented in Section III. Numerical results are illustrated in Section V, and Section VI concludes the paper.

Notation: Scalars and vectors are denoted by lower-case letters and boldface lower-case letters, respectively. For a set $\mathcal{K}$, $|\mathcal{K}|$ denotes its cardinality. For a vector $\mathbf{v}$, $\|\mathbf{v}\|_1$ and $\|\mathbf{v}\|$ denote its ℓ_1 and Euclidean (ℓ_2) norm, respectively. $\mathbb{R}$ represents for the real matrix. $\mathbb{R}^+$ denotes the non-negative real numbers, i.e., $\mathbb{R}^+ = \{x \in \mathbb{R} | x \geq 0\}$. $x \sim \mathcal{CN}(0, \sigma^2)$ represents circularly symmetric complex Gaussian random variable with zero mean and variance σ^2. $\lceil x \rceil$ denotes the ceiling function of x. Finally, $\mathbb{E}[x]$ denotes the expected value of x.

II. System Model and Problem Formulation

We consider a cache-assisted UAV-enabled BackCom network, where a UAV is equipped with a backscatter circuit, namely UAV-enabled backscatter device (UB), to assist the source to transmit data to the destination as shown in Fig. 1.[1] Herein, we assume that the direct transmission link from the source to the destination is impossible due to a heavy obstacle or severe fading. In this work, we focus on communication links between the source to the UB and from the UB to the destination with an assumption that all other users are successfully served by the source through terrestrial communication. Notably, non-terrestrial communication is recognized as a key component to provide cost-effective and high-capacity connectivity in future 5G and beyond/6G wireless networks [46]. The flight altitude of UAV is assumed to be fixed at H meter. We assume the total flying time of UB is T. To make the problem tractable, the time period T is equally divided into N time slots of $\delta_t = T/N$. Consequently, the location of the UAV at time slot n is $\mathbf{q}_n$, with $n \in \mathcal{N} = \{0, \ldots, N\}$. Moreover, the locations of the source and the destination are assumed to be fixed at $\mathbf{w}_s$ and $\mathbf{w}_d$, respectively.

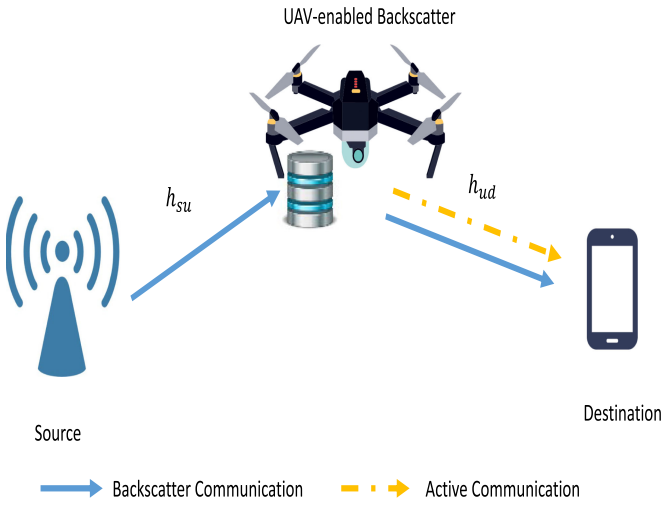

Fig. 1. System model: The cache-aided UAV can perform BackCom and active transmission to convey the data from a source to a destination, wherein the UB is quipped with a energy harvester which harvests energy from the transmit RF signal.

A. Ground-to-Air Channel Model

By denoting V_{max} as a maximum speed of the UB, the UB's constraints can be represented as

$$\|\mathbf{q}_{n+1} - \mathbf{q}_n\| \leq \delta_d = V_{\max}\delta_t, n = 0, \ldots, N-1. \quad (1)$$

$$\mathbf{q}_0 = \mathbf{q}_{\mathrm{I}}, \mathbf{q}_N = \mathbf{q}_{\mathrm{F}}, \quad (2)$$

where $\mathbf{q}_{\mathrm{I}}$ and $\mathbf{q}_{\mathrm{F}}$ is the initial and final location of the UB.

For analytical convenience, let us denote the source, destination, and UB by s, d, and u, respectively. Consequently, the distance from $s \to u$ or $u \to d$ at time slot n is given as

$$d_{iu}^n = \sqrt{H^2 + \|\mathbf{q}_n - \mathbf{w}_i\|^2}, i \in \{s, d\}, \ \forall n, \quad (3)$$

where $\mathbf{w}_s$ and $\mathbf{w}_d$ are fixed locations of the source and destination.

This work considers a realistic channel model consisting of both line-of-sight (LOS) and non-line-of-sight (NLOS) channel. This is because the UB can operate in different environments, e.g., urban, sub-urban, or rural area. Particularly, we take large-scale fading and small-scale fading into consideration [3], [47].

[1] In the case that one UAV serves multiple ground users (GUs), each user may request different content. Therefore, we need to optimize the bandwidth and power allocation for each GU k to prevent co-channel interference and overcome the UAV's power limitation. In this context, our formulated problem is to maximize the total achievable throughput at the destination by jointly optimizing the dynamic time splitting (DTS) ratio, UAV trajectory, and resource allocations (i.e., bandwidth and power allocation). Therefore, the block coordinate descent (BCS) method presented in section III can still be applied to solve the new formulated problem by decomposing the proposed problem into three sub-problems. The solutions of the first (i.e., optimize the DTS ratio) and second sub-problem (i.e., optimize the UAV trajectory) can be obtained as in the manuscript. The solution of the third sub-problem (i.e., optimize the UAV resources) can be obtained similar to [45, Section III-C].

Concretely, the channel coefficient h_{iu}^n at time slot n is given as

$$h_{iu}^n = \sqrt{\psi_{iu}^n}\tilde{h}_{iu}^n, \tag{4}$$

where ψ_{iu}^n and $\tilde{h}_{iu}^n$ denotes the large-scale fading and small-scale fading during time slot n, respectively. Specifically, $\psi_{iu}[n]$ can be written as

$$\psi_{iu}^n = \omega_0 (d_{iu}^n)^{-\alpha}, \tag{5}$$

where ω_0 represents the reference channel gain at $d_{iu} = 1$ meter, and α denotes the path loss exponent. The small-scale fading $\tilde{h}_{iu}^n$ with $\mathbb{E}[|\tilde{h}_{iu}^n|^2] = 1$, can be modeled as

$$\tilde{h}_{iu}^n = \sqrt{\frac{K}{1+K}}\bar{h}_{iu}^n + \sqrt{\frac{1}{1+K}}\hat{h}_{iu}^n, \tag{6}$$

where $\bar{h}_{iu}^n$ accounts for deterministic LoS, $\hat{h}_{iu}^n$ denotes the NLoS component, and K is the Rician factor.

B. Caching Model

We consider a general caching model at the UB, whereas the UB needs to retrieve the information from its cache to serve the destination. Specifically, the UB is able to store $0 \leq \sigma \leq 1$ parts of each file in its cache.[2] Henceforth, σ is considered as the caching coefficient in this paper. When the destination requests a file, a part σ of this file is already stored in the UB's storage. Therefore, the source only needs to send the remainder of the required file to the UB before its transmission to the destination via backscatter. Moreover, the caching scheme adopted in this work can be considered as a lower bound method in comparison with the case when UB knew the content popularity.

C. Energy Harvesting and Energy Consumption Constraints

Due to the limited energy storage at the UB, EH becomes a promising solution in prolonging the lifetime of the UB. We design a dynamic time-splitting mechanism wherein the UB communication can be divided into two dynamic phases within a time slot. Specifically, a fraction τ_n and $(1-\tau_n)$ of duration δ_t are used for backscattering signal and EH at the UB, respectively. In the second phase of $(1-\tau_n)\delta_t$, the harvested energy expression at the UB at time slot n is given by [48].

$$E_h^n = E_{\mathrm{L}}^n \triangleq \mu(1-\tau_n)\delta_t P_{\mathrm{WPT}}\mathbb{E}[|h_{su}^n|^2], \tag{7}$$

where P_{WPT} is the transmit power at the source during $(1-\tau_n)\delta_t$ of n-th time slot, E_{L}^n is the harvested energy, μ denotes the energy harvesting efficiency corresponding to the LEH model and τ_n represents the DTS ratio at time slot n. More specifically, $\tau_n = 1$ means that all the signal is backscattered to the receiver during time slot n and $\tau_n = 0$ indicates that all the signal is used for EH. Furthermore, ϕ is defined as $\phi \triangleq \frac{1}{1+e^{\beta\nu}}$, wherein β and ν are constant values with regards to circuit specifications such as diode turn-on voltage, capacitance, and resistance. Ξ is the maximum harvested power at the UB when the EH circuit is saturated.

The energy consumption of UAV consists of three parts: energy consumption due to propulsion, backscatter, and active communications. Specifically, the propulsion energy consumption of UAV during time slot n can be represented as [3], [5]

$$E_{\mathrm{fly}}^n(\mathbf{q}) = P_0\left(\delta_t + \kappa_1\Delta_n^2\right) + P_1\sqrt{\sqrt{\delta_t^4 + \kappa_2^2\Delta_n^4} - \kappa_2\Delta_n^2} + \frac{\kappa_3\Delta_n^3}{\delta_t^2}, \tag{8}$$

where $\Delta_n \triangleq \|\mathbf{q}_{n+1} - \mathbf{q}_n\|$, $P_0 \triangleq \frac{\delta}{8}\rho s A\Omega^3 R^3$, $P_1 = (1+I)\frac{W^{3/2}}{\sqrt{2\rho A}}$, $\kappa_1 = \frac{3}{\Omega^2 R^2}$, $\kappa_2 = \frac{1}{2v_0^2}$, and $\kappa_3 = 0.5 d_0 \rho s A$, with $I = 0.1$ is the incremental correction factor to induced power and other parameters can be explained as in Table I of [5].

The energy consumption due to BackCom during time slot n is represented as $\tau_n\delta_t P_b$, where P_b is the circuit power of the UB during backscatter period [48]. Moreover, P_u^n denote the transmit power of UAV during time slot n for data transmission. We then have the following energy constraint

$$\sum_{i=1}^{n}\left(E_{\mathrm{fly}}^n(\mathbf{q}) + \tau_n\delta_t\left(P_b + P_u\right)\right) \leq \sum_{i=1}^{n} E_h^n, \tag{9}$$

where the constraint (9) guarantees that the total UAV's energy consumption should be less than or equal to the summation of harvested energy of the UB until time slot $n \in \mathcal{N}$.

By substituting (7) into (9), we have

$$\sum_{i=1}^{n}\left(E_{\mathrm{fly}}^n(\mathbf{q}) + \tau_n\delta_t\left(P_b + P_u\right)\right) \leq \sum_{i=1}^{n}\frac{\mu(1-\tau_n)\delta_t\omega_0 P_{\mathrm{WPT}}}{\left(H^2 + \|\mathbf{q}_n - \mathbf{w}_s\|^2\right)^{\alpha/2}}, \tag{10}$$

where $\mathbb{E}[h_{su}^n] = \frac{\omega_0}{(H^2+\|\mathbf{q}_n-\mathbf{w}_s\|^2)^{\alpha/2}}$.

TABLE I
SIMULATION PARAMETERS

Parameters	Values
UAV's altitude, H	10 meters [8]
Maximum speed, $V_{\max}$	20 m/s [8]
Noise power, σ^2	-90 dB [8]
Path loss exponent, α	2.3 [7]
Backscatter circuit power consumption P_b	$10^{-6}W$ [59]
Channel power gain at reference distance, ω_0	-30 dB [8]
Time slot duration, δ_t	0.5 second
Error tolerance threshold, ϵ	10^{-4}
Energy harvesting coefficient, μ	0.84 [60]
Maximum backscatter coefficient, $\eta_{\max}$	0.5 [49]
Source's transmit power for information transmission, P_s	16 dBm
Source's transmit power for charging the UAV, P_{WPT}	[27,40] dB [34]
Demanded data of the destination, S	50 Mbits
Error tolerance, ϵ	10^{-4}

D. UAV-Enabled Backscatter (UB)

In this work, we consider a UB as a flying backscatter device to reflect the signal from source to destination. To avoid the co-channel interference on the uplink (UL) and downlink (DL), time-division duplexing (TDD) is utilized in this system [8]. Specifically, we consider DTS method to divide each time slot into two parts. In this context, $(1-\tau_n)\delta_t$ and $\tau_n\delta_t$ are the

[2]This caching method is also known as probabilistic caching.

fraction of time for data transmission on the UL from $s \to u$ and the DL from $u \to d$, respectively, where $0 \le \tau_n \le 1$ denotes the DTS ratio at the time slot n.

Let us denote the symbol transmitted from the source during time slot n by x_s^n with unit power $\mathbb{E}[|x_s^n|^2] = 1$. Then, the received signal at the UB during time slot n is given by

$$y_u^n = \sqrt{P_s} h_{su}^n x_s^n + n_u, \tag{11}$$

where P_s is the transmit power of source S used for information transmission, and $n_u \sim \mathcal{CN}(0, \sigma_u^2)$ denotes the additive white Gaussian noise (AWGN) at the UB. Let us denote x_u^n as the backscatter information signal at time slot n, the transmitted signal of the UB is then given as [49]

$$x_u^n = \sqrt{\eta_u^n P_s} h_{su}^n x_s^n, \tag{12}$$

where η_u^n represents the backscatter coefficient during time slot n. Since η_u^n can not reach 1 in practice due to material and circuit losses [49]. Hence, we set a threshold for $\eta_u^n \le \eta_{\max}$, with $0 < \eta_{\max} < 1$. Moreover, the additional noise and signal processing delay are ignored in (12) which are widely utilized in [48]–[50]. Consequently, the received signal at destination during time slot n is given as

$$y_d^n = h_{ud}^n x_u^n + \sqrt{P_u} h_{ud}^n x_s^n + n_d, \tag{13}$$

where the first and second element represent the received signal at the destination due to backscattering and active data transmission; $n_d \sim \mathcal{CN}(0, \sigma_d^2)$ denote the additive white Gaussian noise (AWGN) at the destination. Note that the backscatter noise power, i.e, $\sqrt{\eta_u^n n_u}$, is much smaller than baseband noise power [51], thus it is eliminated from (13). By substituting (12) into (13), we have

$$y_d^n = \underbrace{h_{ud}^n x_u^n}_{\text{Information from S}} + \underbrace{\lceil \sigma \rceil \sqrt{P_u} h_{ud}^n x_{\text{cache}}^n}_{\text{Cached information}} + n_d, \tag{14}$$

where x_{cache}^n denotes a fraction of requested information that was cached at the UAV. $\sqrt{P_s} h_{ud}^n x_s^n$ and $\sqrt{P_u} h_{ud}^n x_s^n$ are the backscattering and active RF signal to transmit received signal from source S during time slot n. Moreover, $\lceil \sigma \rceil \sqrt{P_u} h_{ud}^n x_{\text{cache}}^n$ means that if the UAV has cached a σ fraction of the requested file in its storage, thus it can transmit the cached signal to the destination. Further, n_d is the noise power at the destination which is an independent and identically distributed (i.i.d.) complex Gaussian random variable with zero mean and variance σ_d^2. Thus, the SNR at the destination are represented as

$$\gamma_d^n = \frac{\eta_u^n P_s |h_{su}^n|^2 |h_{ud}^n|^2 + P_u \lceil \sigma \rceil |h_{ud}^n|^2}{\sigma_d^2}, \tag{15}$$

Then, the achievable rate (in bps) at the UB and the destination during time slot n can be respectively calculated as

$$R_u^n = B \log_2 \left(1 + \gamma_u^n\right), \tag{16}$$

$$R_d^n = B \log_2 \left(1 + \gamma_d^n\right), \tag{17}$$

where B denotes the sytem bandwidth in hertz (Hz); $\gamma_u^n = P_s |h_{su}^n|^2 / \sigma_u^2$, B is the total bandwidth. Especially, the instantaneous channel state information (CSI) (i.e., h_{su}^n and h_{ud}^n) are random variables, thus the instantaneous rate is also a random variable. Thus, the approximated received rate of the UB and the destination are adopted, which can be expressed as [8]

$$\bar{R}_u^n = B \mathbb{E}[\log_2 (1 + \gamma_u^n)], \tag{18}$$

$$\bar{R}_d^n = B \mathbb{E}[\log_2 (1 + \gamma_d^n)]). \tag{19}$$

As explicit, it is difficult to obtain the closed-form expression of $\bar{R}_u^n$ and $\bar{R}_d^n$, and hence the approximation functions for $\bar{R}_u^n$ and $\bar{R}_d^n$ are expressed as in the following lemma:

Lemma 1: The approximation expressions of $\bar{R}_u^n$ and $\bar{R}_d^n$ are respectively given as

$$\bar{R}_u^n = B \log_2 \left(1 + \frac{e^{-E} \omega_0 P_s}{\left(H^2 + \|\mathbf{q}_n - \mathbf{w}_s\|^2\right)^{\alpha/2} \sigma_u^2}\right), \tag{20}$$

$$\bar{R}_d^n = B \log_2 \left(1 + \frac{\Theta \left(\eta_u^n \omega_0 P_s + P_u \lceil \sigma \rceil \left(d_{su}^n\right)^{\alpha}\right)}{\varrho}\right), \tag{21}$$

where $\Theta \triangleq \frac{e^{-E}\omega_0}{\sigma_d^2}$, $\bar{P}_u \triangleq P_u \lceil \sigma \rceil$, $\varrho \triangleq (H^2 + \|\mathbf{q}_n - \mathbf{w}_s\|^2)^{\alpha/2} (H^2 + \|\mathbf{q}_n - \mathbf{w}_d\|^2)^{\alpha/2}$.

Proof: See Appendix A. ∎

E. Problem Formulation

This section aims at maximizing the total data transmission from $u \to d$ by jointly optimizing the DTS ratio and UB trajectory with consideration of a linear EH model. Let us define $\mathbf{q} \triangleq \{\mathbf{q}_n, n \in \mathcal{N}\}$, $\boldsymbol{\tau} \triangleq \{\tau_n, n \in \mathcal{N}\}$. Then, the problem is mathematically formulated as follows

$$\mathcal{P}_1: \max_{\mathbf{q}, \boldsymbol{\tau}} B \sum_{n \in \mathcal{N}} \tau_n \delta_t \log_2 \left(1 + \frac{\Theta \left(\eta_u^n \omega_0 P_s + \bar{P}_u \left(d_{su}^n\right)^{\alpha}\right)}{\varrho}\right) \tag{22a}$$

s.t.

$$B \sum_{n \in \mathcal{N}} \tau_n \delta_t \log_2 \left(1 + \frac{e^{-E} \omega_0 P_s}{\left(H^2 + \|\mathbf{q}_n - \mathbf{w}_s\|^2\right)^{\alpha/2} \sigma_u^2}\right) + \sigma S \ge B \sum_{n \in \mathcal{N}} \tau_n \delta_t \log_2 \left(1 + \frac{\Theta \left(\eta_u^n \omega_0 P_s + \bar{P}_u \left(d_{su}^n\right)^{\alpha}\right)}{\varrho}\right), \tag{22b}$$

$$B \sum_{n \in \mathcal{N}} \tau_n \delta_t \log_2 \left(1 + \frac{\Theta \left(\eta_u^n \omega_0 P_s + \bar{P}_u \left(d_{su}^n\right)^{\alpha}\right)}{\varrho}\right) \ge S, \tag{22c}$$

$$\sum_{i=1}^{n} \left(E_{\text{fly}}^n(\mathbf{q}) + \tau_n \delta_t \left(P_b + P_u\right)\right) \le \sum_{i=1}^{n} \frac{\mu (1 - \tau_n) \delta_t \omega_0 P_{\text{WPT}}}{\left(H^2 + \|\mathbf{q}_n - \mathbf{w}_s\|^2\right)^{\alpha/2}}, \tag{22d}$$

$$\|\mathbf{q}_{n+1} - \mathbf{q}_n\| \le \delta_d = V_{\max} \delta_t, n = 0, \ldots, N-1, \tag{22e}$$

$$\mathbf{q}_0 = \mathbf{q}_{\text{I}}, \mathbf{q}_N = \mathbf{q}_{\text{F}}, \tag{22f}$$

$$0 \le \tau_n \le 1, n \in \mathcal{N}, \tag{22g}$$

where S is the demanded data (in bits) by the destination; constraint (22a) guarantees a non-empty caching at the UB; constraint eq:P1 means that the total transmitted data on the DL from $u \rightarrow d$ should be larger than or equal to the demanded data of the destination; constraint (22a) implies that the DTS ratio value must be less than or equal to 1.

The problem $\mathcal{P}_1$ is a non-convex problem, which is NP-hard. Specifically, the objective function, constraints (22a), eq:P1, (22a) are non-convex. Thus, it is troublesome to find the direct solution of $\mathcal{P}_1$. In the succeeding section, we introduce an efficient method to solve it.

III. Proposed Alternating Algorithm for Solving $\mathcal{P}_1$

To tackle the non-convexity of the problem $\mathcal{P}_1$, we first decompose $\mathcal{P}_1$ into two sub-problems, wherein we first target the optimization of DTS ratio for a given trajectory, and we perform the trajectory optimization for a given DTS ratio. By employing the block coordinate descent (BCD) method [52], we propose an efficient iterative algorithm wherein we alternately optimize three subproblems until the algorithm converges to a given threshold, $\epsilon > 0$.

A. Dynamic Time Splitting Ratio Optimization:

For any given UB trajectory $\mathbf{q}$, the DTS ratio $\boldsymbol{\tau}$ can be obtained by solving the following optimization problem:

$$\mathcal{P}_1^{\boldsymbol{\tau}}: \max_{\boldsymbol{\tau}} \sum_{n\in\mathcal{N}} \tau_n \delta_t \bar{R}_d^n \tag{23a}$$

$$\text{s.t.} \sum_{n\in\mathcal{N}} \tau_n \delta_t \bar{R}_u^n + \sigma S \geq \sum_{n\in\mathcal{N}} \tau_n \delta_t \bar{R}_d^n,$$

$$\sum_{n\in\mathcal{N}} \tau_n \delta_t \bar{R}_d^n \geq S, \tag{23b}$$

$$\sum_{i=1}^{n} \left(E_{\text{fly}}^n(\mathbf{q}) + \tau_n \delta_t \left(P_b + P_u\right)\right) \leq \sum_{i=1}^{n} \frac{\mu(1-\tau_n)\delta_t \omega_0 P_{\text{WPT}}}{\left(H^2 + \|\mathbf{q}_n - \mathbf{w}_s\|^2\right)^{\alpha/2}}, \tag{23c}$$

$$0 \leq \tau_n \leq 1, n \in \mathcal{N}. \tag{23d}$$

It is clear that $\mathcal{P}_1^{\boldsymbol{\tau}}$ is a linear optimization problem, and hence is convex. Moreover, it is easy to verify that the Slater's condition holds for $\mathcal{P}_1^{\boldsymbol{\tau}}$ and thus the KKT conditions are sufficient for optimality [53, Section 5.5]. Then, the Lagrangian function corresponding to problem $\mathcal{P}_1^{\boldsymbol{\tau}}$ is expressed as

$$\mathcal{L}(\boldsymbol{\tau}, \lambda_1, \lambda_2, \lambda_3, \lambda_4) \triangleq F(\tau) + \lambda_1 G(\boldsymbol{\tau}) + \lambda_2 H(\boldsymbol{\tau}) + \lambda_3 I(\boldsymbol{\tau}) + \lambda_4 J(\boldsymbol{\tau}), \tag{24}$$

with

$$F(\boldsymbol{\tau}) \triangleq \sum_{n\in\mathcal{N}} \tau_n \delta_t \bar{R}_d^n \tag{25}$$

$$G(\boldsymbol{\tau}) \triangleq \left(\sum_{n\in\mathcal{N}} \tau_n \delta_t \bar{R}_u^n + \sigma S - \sum_{n\in\mathcal{N}} \tau_n \delta_t \bar{R}_d^n\right) \geq 0 \tag{26}$$

$$H(\boldsymbol{\tau}) \triangleq \sum_{n\in\mathcal{N}} \tau_n \delta_t \bar{R}_d^n - S \geq 0, \tag{27}$$

$$I(\boldsymbol{\tau}) \triangleq \sum_{i=1}^{n} \chi_1 (1-\tau_n) - \sum_{i=1}^{n} \left(E_{\text{fly}}^n(\mathbf{q}) + \tau_n \delta_t \left(P_b + P_u\right)\right) \geq 0, \tag{28}$$

$$J(\boldsymbol{\tau}) \triangleq 1 - \tau_n \geq 0. \tag{29}$$

where λ_1, λ_2, λ_3, λ_4 is the Lagrangian dual variables; $\chi_1 \triangleq \frac{\mu \delta_t \omega_0 P_{\text{WPT}}}{(H^2 + \|\mathbf{q}_n - \mathbf{w}_s\|^2)^{\alpha/2}}$.

The stationarity condition is given as

$$\frac{\partial \mathcal{L}(\boldsymbol{\tau}, \lambda_1, \lambda_2, \lambda_3, \lambda_4)}{\partial \boldsymbol{\tau}} = \sum_{n\in\mathcal{N}} \delta_t \bar{R}_d^n + \lambda_1 \left(\sum_{n\in\mathcal{N}} \delta_t \bar{R}_u^n - \sum_{n\in\mathcal{N}} \delta_t \bar{R}_d^n\right) + \lambda_2 \sum_{n\in\mathcal{N}} \delta_t \bar{R}_d^n - \lambda_3 \left(\sum_{n\in\mathcal{N}} \chi_1 + \sum_{n\in\mathcal{N}} \delta_t \left(P_b + P_u\right)\right) - \lambda_4 = 0. \tag{30}$$

The conditions for primal feasibility are given as (26), (27), (28), and (29). Then, the complementary slackness conditions can be expressed as follows

$$\lambda_1 G(\boldsymbol{\tau}) = 0, \tag{31}$$

$$\lambda_2 H(\boldsymbol{\tau}) = 0, \tag{32}$$

$$\lambda_3 I(\boldsymbol{\tau}) = 0, \tag{33}$$

$$\lambda_4 J(\boldsymbol{\tau}) = 0. \tag{34}$$

Furthermore, the dual feasibility conditions should hold $\lambda_1, \lambda_2, \lambda_3, \lambda_4 \geq 0$. The solution is then postulated in the following theorem.

Theorem 1: The optimal value $\{\tau_n^\star\}$ to problem $\mathcal{P}_1^{\boldsymbol{\tau}}$ can be expressed as

$$\tau_n^\star = \begin{cases} \left[\frac{\sigma S}{N\delta_t(\bar{R}_d^n - \bar{R}_u^n)}\right]_0^1, \text{ iff } \bar{R}_d^n > \bar{R}_u^n, \forall n \in \mathcal{N} & \text{(35a)} \\ \left[\frac{\chi_1 - E_{\text{fly}}^n(\mathbf{q})}{\chi_1 + \delta_t(P_b + P_u)}\right]_0^1. & \text{(35b)} \end{cases}$$

From Eq. (35), we report two possible solutions of $\{\tau_n^\star\}$. In order to reach to an optimal outcome, we select the best solution that maximizes the objective function in $\mathcal{P}_1^{\tau}$. Particularly, the optimal value of $\{\tau_n^\star\}$ from (35b) must be guaranteed to be inside the feasible set, i.e., $0 \leq \tau_n \leq 1$.

Proof: See Appendix B. ■

B. Trajectory Optimization:

For given values of $\boldsymbol{\tau}$, the UAV trajectory $\mathbf{q}$ can be achieved by solving the following problem

$$\mathcal{P}_1^{\mathbf{q}}: \max_{\mathbf{q}} B \sum_{n\in\mathcal{N}} \tau_n \delta_t \log_2 \left(1 + \frac{\Theta\left(\eta_u^n \omega_0 P_s + \bar{P}_u \left(d_{su}^n\right)^\alpha\right)}{\varrho}\right) \tag{36a}$$

s.t.

$$B\sum_{n\in\mathcal{N}}\tau_n\delta_t\log_2\left(1+\frac{e^{-E}\omega_0 P_s^n}{\left(H^2+\|\mathbf{q}_n-\mathbf{w}_s\|^2\right)^{\alpha/2}\sigma_u^2}\right)+\sigma S$$
$$\geq B\sum_{n\in\mathcal{N}}\tau_n\delta_t\log_2\left(1+\frac{\Theta\left(\eta_u^n\omega_0 P_s+\bar{P}_u\left(d_{su}^n\right)^{\alpha}\right)}{\varrho}\right), \tag{36b}$$

$$B\sum_{n\in\mathcal{N}}\tau_n\delta_t\log_2\left(1+\frac{\Theta\left(\eta_u^n\omega_0 P_s+\bar{P}_u\left(d_{su}^n\right)^{\alpha}\right)}{\varrho}\right)\geq S, \tag{36c}$$

$$\sum_{i=1}^{n}\left(E_{\text{fly}}^n(\mathbf{q})+\tau_n\delta_t\left(P_b+P_u\right)\right)$$
$$\leq\sum_{i=1}^{n}\frac{\mu(1-\tau_n)\delta_t\omega_0 P_{\text{WPT}}}{\left(H^2+\|\mathbf{q}_n-\mathbf{w}_s\|^2\right)^{\alpha/2}}, \tag{36d}$$

$$(22e),(22f), \tag{36e}$$

The problem $\mathcal{P}_1^{\mathbf{q}}$ is still non-convex, which is difficult to efficiently solve by utilizing standard optimization methods. To make $\mathcal{P}_1^{\mathbf{q}}$ more tractable, we firstly introduce slack variables z_1^n and z_2^n such that $(H^2+\|\mathbf{q}_n-\mathbf{w}_s\|^2)\leq(z_1^n)^{2/\alpha}$ and $(H^2+\|\mathbf{q}_n-\mathbf{w}_d\|^2)\leq(z_2^n)^{2/\alpha}$, respectively. Let us denote $\mathbf{z}\triangleq\{z_1^n,z_2^n,n\in\mathcal{N}\}$, by which the problem $\mathcal{P}_1^{\mathbf{q}}$ is rewritten as

$$\mathcal{P}_{1.1}^{\mathbf{q}}:\max_{\mathbf{q},\mathbf{z}}B\sum_{n\in\mathcal{N}}\tau_n\delta_t\log_2\left(1+\frac{\Theta\left(\eta_u^n\omega_0 P_s+\bar{P}_u z_1^n\right)}{z_1^n z_2^n}\right) \tag{37a}$$

$$\text{s.t.}\left(H^2+\|\mathbf{q}_n-\mathbf{w}_s\|^2\right)\leq(z_1^n)^{2/\alpha}, \tag{37b}$$

$$\left(H^2+\|\mathbf{q}_n-\mathbf{w}_d\|^2\right)\leq(z_2^n)^{2/\alpha}, \tag{37c}$$

$$B\sum_{n\in\mathcal{N}}\tau_n\delta_t\log_2\left(1+\frac{e^{-E}\omega_0 P_s^n}{z_1^n\sigma_u^2}\right)+\sigma S$$
$$\geq B\sum_{n\in\mathcal{N}}\tau_n\delta_t\log_2\left(1+\frac{\Theta\left(\eta_u^n\omega_0 P_s+\bar{P}_u z_1^n\right)}{z_1^n z_2^n}\right), \tag{37d}$$

$$B\sum_{n\in\mathcal{N}}\tau_n\delta_t\log_2\left(1+\frac{\Theta\left(\eta_u^n\omega_0 P_s+\bar{P}_u z_1^n\right)}{z_1^n z_2^n}\right)\geq S, \tag{37e}$$

$$\sum_{i=1}^{n}\left(E_{\text{fly}}^n(\mathbf{q})+\tau_n\delta_t\left(P_b+P_u\right)\right)$$
$$\leq\sum_{i=1}^{n}\frac{\mu(1-\tau_n)\delta_t\omega_0 P_{\text{WPT}}}{z_1^n}, \tag{37f}$$

$$(22e),(22f), \tag{37g}$$

Note that the problem $\mathcal{P}_{1.1}^{\mathbf{q}}$ is simpler than $\mathcal{P}_1^{\mathbf{q}}$, but it is still difficult to be directly solved. This is because the objective function is convex and the non-convexity of constraints (37a), (37a), and (37a). In the following, we transform $\mathcal{P}_{1.1}^{\mathbf{q}}$ into a convex form by introducing the following lemmas:

Lemma 2: For any given $z_1^{n,j}$ and $z_2^{n,j}$ at j-th iteration, $\log_2(1+\frac{e^{-E}\omega_0 P_s^n}{z_1^n\sigma_u^2})$ and $\log_2(1+\frac{\Theta(\eta_u^n\omega_0 P_s+\bar{P}_u z_1^n)}{z_1^n z_2^n})$ are respectively lower bounded by

$$\log_2\left(1+\frac{e^{-E}\omega_0 P_s}{z_1^n\sigma_u^2}\right)\geq\log_2\left(1+\frac{e^{-E}\omega_0 P_s}{z_1^{n,j}\sigma_u^2}\right)$$
$$-\frac{e^{-E}\omega_0 P_s(z_1^n-z_1^{n,j})}{z_1^{n,j}(z_1^{n,j}\sigma_u^2+e^{-E}\omega_0 P_s)\ln 2}\triangleq\Theta_1, \tag{38}$$

$$\log_2\left(1+\frac{\Theta\left(\eta_u^n\omega_0 P_s+\bar{P}_u z_1^n\right)}{z_1^n z_2^n}\right)$$
$$\geq\log_2\left(1+\frac{\Theta\left(\eta_u^n\omega_0 P_s+\bar{P}_u z_1^{n,j}\right)}{z_1^{n,j}z_2^{n,j}}\right)$$
$$-\frac{\Theta\eta_u^n\omega_0 P_s(z_1^n-z_1^{n,j})}{z_1^{n,j}\left(\Theta\eta_u^n\omega_0 P_s+z_1^{n,j}(\Theta\bar{P}_u+z_2^{n,j})\right)\ln 2}$$
$$-\frac{\Theta\left(\eta_u^n\omega_0 P_s+\bar{P}_u z_1^{n,j}\right)(z_2^n-z_2^{n,j})}{z_2^{n,j}\left(\Theta\eta_u^n\omega_0 P_s+z_1^{n,j}(\Theta\bar{P}_u+z_2^{n,j})\right)\ln 2}\triangleq\Theta_2. \tag{39}$$

Proof: It is observed that $\log_2(1+1/x)$ and $\log_2(1+(A_2+A_3x)/xy)$ are convex functions, with $x>0$ and $y>0$, see Appendix C. Then, we adopt the first-order Taylor approximation to respectively approximate above convex functions at any given feasible points x^j, y^j as

$$\log_2\left(1+\frac{A_1}{x}\right)\geq\log_2\left(1+\frac{A_1}{x^j}\right)$$
$$-\frac{A_1}{x^j(x^j+A_1)\ln 2}(x-x^j), \tag{40}$$

$$\log_2\left(1+\frac{A_2+A_3x}{xy}\right)\geq\log_2\left(1+\frac{A_2+A_3x^j}{x^j y^j}\right)$$
$$-\frac{A_2(x-x^j)}{x^j\left(A_2+x^j(A_3+y^j)\right)\ln 2}$$
$$-\frac{\left(A_2+A_3x^j\right)(y-y^j)}{y^j\left(A_2+x^j(A_3+y^j)\right)\ln 2}. \tag{41}$$

By applying $A_1\triangleq e^{-E}\omega P_s$, $x\triangleq z_1^n$, $y\triangleq z_2^n$, $A_2\triangleq\Theta\eta_u^n\omega_0 P_s$, and $A_3\triangleq\Theta P_u$ then the Lemma 2 is proved. ■

Lemma 3: For any given $z_1^{n,j}$ at the j-th iteration, the lower bound of $1/z_1^n$ can be expressed as

$$\frac{1}{z_1^n}\geq\frac{1}{z_1^{n,j}}-\frac{1}{(z_1^{n,j})^2}(z_1^n-z_1^{n,j})\triangleq\tilde{z}_1^n. \tag{42}$$

Then, we obtain the following optimization problem:

$$\mathcal{P}_{1.2}^{\mathbf{q}}: \max_{\mathbf{q},\mathbf{z}} B\sum_{n\in\mathcal{N}}\tau_n\delta_t\Theta_2 \tag{43a}$$

$$\text{s.t. } (22\text{e}),(22\text{f}),(37\text{b}),(37\text{c}), \tag{43b}$$

$$B\sum_{n\in\mathcal{N}}\tau_n\delta_t\Theta_1+\sigma S\geq B\sum_{n\in\mathcal{N}}\tau_n\delta_t\Theta_2, \tag{43c}$$

$$B\sum_{n\in\mathcal{N}}\tau_n\delta_t\Theta_2\geq S, \tag{43d}$$

$$\sum_{i=1}^{n}\left(E_{\text{fly}}^{n}(\mathbf{q})+\tau_n\delta_t\left(P_b+P_u\right)\right)\leq\sum_{i=1}^{n}\mu(1-\tau_n)\delta_t\omega_0P_{\text{WPT}}\tilde{z}_1^n. \tag{43e}$$

The problem $\mathcal{P}_{1.2}^{\mathbf{q}}$ is still non-convex due to the second term of $E_{\text{fly}}^{n}(\mathbf{q})$ (8). To tackle this issue, we introduce slack variable y_n, such that

$$\sqrt{\delta_t^4+\kappa_2^2\Delta_n^4}-\kappa_2\Delta_n^2\leq y_n^2,\forall n\in\mathcal{N}. \tag{44}$$

After some manipulations, it yields

$$\frac{\delta_n^4}{y_n^2}\leq y_n^2+2\kappa_2\Delta_n^2. \tag{45}$$

Consequently, the second term of $E_{\text{fly}}^{n}(\mathbf{q})$ can be substituted by P_1y_n and $E_{\text{fly}}^{n}(\mathbf{q})$ is replaced by its upper bound

$$E_{\text{fly}}^{n}(\mathbf{q})\leq P_0\left(\delta_t+\kappa_1\Delta_n^2\right)+P_1y_n+\frac{\kappa_3\Delta_n^3}{\delta_t^2}\triangleq\bar{E}_{\text{fly}}^{n}(\mathbf{q}), \tag{46}$$

With the above manipulations, $\mathcal{P}_{1.3}^{\mathbf{q}}$ can be re-written as

$$\mathcal{P}_{1.3}^{\mathbf{q}}: \max_{\mathbf{q},\mathbf{z}} B\sum_{n\in\mathcal{N}}\tau_n\delta_t\Theta_2 \tag{47a}$$

$$\text{s.t. } (22\text{e}),(22\text{f}),(37\text{b}),(37\text{c}),(43\text{c}),(43\text{d}), \tag{47b}$$

$$\sum_{i=1}^{n}\left(\bar{E}_{\text{fly}}^{n}(\mathbf{q})+\tau_n\delta_t\left(P_b+P_u\right)\right)\leq\sum_{i=1}^{n}\mu(1-\tau_n)\delta_t\omega_0P_{\text{WPT}}\tilde{z}_1^n \tag{47c}$$

$$\frac{\delta_n^4}{y_n^2}\leq y_n^2+2\kappa_2\left\|\mathbf{q}_{n+1}-\mathbf{q}_n\right\|^2,\forall n \tag{47d}$$

The problem $\mathcal{P}_{1.3}^{\mathbf{q}}$ is still non-convex due to non-convex constraint (47d). Thus, we apply first-order Taylor to convexify (47d) as follows

$$\frac{\delta_n^4}{y_n^2}\leq(y_n^j)^2+2y_n^j\left(y_n-y_n^j\right)-2\kappa_2\left\|\mathbf{q}_{n+1}^j-\mathbf{q}_n^j\right\|^2+4\kappa_2\left(\mathbf{q}_{n+1}^j-\mathbf{q}_n^j\right)^T\left(\mathbf{q}_{n+1}-\mathbf{q}_n\right),\forall n. \tag{48}$$

Algorithm 1: Proposed BCD-Based Algorithm to Solve $\mathcal{P}_1$.

Initialization: Set $j:=0$ and initialize $\mathbf{q}^j$, $\boldsymbol{\tau}^j$.
1: **repeat**
2: Solve $\mathcal{P}_1^{\boldsymbol{\tau}}$ for given $\{\mathbf{q}^j\}$ and denote the optimal solution as $\boldsymbol{\tau}^\star$.
3: Solve $\mathcal{P}_1^{\mathbf{q}}$ for given $\{\boldsymbol{\tau}^{j+1}\}$ and denote the optimal solution as $\mathbf{q}^\star$.
4: Update the local point $\boldsymbol{\tau}^{j+1}=\boldsymbol{\tau}^\star$ and $\mathbf{q}^{j+1}=\mathbf{q}^\star$.
5: Set $j:=j+1$.
6: **until** Convergence

Bearing all the above discussions in mind, we solve the following approximate convex problem at the j-th iteration:

$$\mathcal{P}_{1.4}^{\mathbf{q}}: \max_{\mathbf{q},\mathbf{z}} B\sum_{n\in\mathcal{N}}\tau_n\delta_t\Theta_2 \tag{49a}$$

$$\text{s.t.}$$

$$(22\text{e}),(22\text{f}),(37\text{b}),(37\text{c}),(43\text{d}),(47\text{c}), \tag{49b}$$

$$\frac{\delta_n^4}{y_n^2}\leq(y_n^j)^2+2y_n^j\left(y_n-y_n^j\right)-2\kappa_2\left\|\mathbf{q}_{n+1}^j-\mathbf{q}_n^j\right\|^2+4\kappa_2\left(\mathbf{q}_{n+1}^j-\mathbf{q}_n^j\right)^T\left(\mathbf{q}_{n+1}-\mathbf{q}_n\right),\forall n. \tag{49c}$$

Since the objective function and all constraints pf $\mathcal{P}_{1.4}^{\mathbf{q}}$ are convex, thus it can be directly solved by applying standard optimization methods [53]. To this end, we propose an iterative algorithm based on the solutions of three sub-problems. The alternating algorithm is summarized as in Algorithm 1.

To ensure the feasibility of Algorithm 1, an appropriate initial point is required. In our setup, we set $\eta_u^{n,j}=\eta_{\max}$, $\tau_{n,j}=0.5$. Notably, the convergence of Algorithm 1 depends on the initial trajectory. The initial UAV trajectory should be selected such that the feasibility of (47c) is fulfilled while also guaranteeing other constraints. Thus, we can obtain $\mathbf{q}^j$ by solving the simplified version of $\mathcal{P}_{1.4}^{\mathbf{q}}$ as follows

$$\mathcal{P}_{\text{feasible}}^{\mathbf{q}}: \max_{\mathbf{q},\{\zeta_n\}_{n=1}^N}\min_{n\in\mathcal{N}}\zeta_n \tag{50a}$$

$$\text{s.t.}$$

$$(22\text{e}),(22\text{f}),(37\text{b}),(37\text{c}),(43\text{c}),(43\text{d}),(49\text{c}), \tag{50b}$$

$$\sum_{i=1}^{n}\mu(1-\tau_n)\delta_t\omega_0P_{\text{WPT}}\tilde{z}_1^n-\sum_{i=1}^{n}\left(\bar{E}_{\text{fly}}^{n}(\mathbf{q})+\tau_n\delta_t\left(P_b+P_u\right)\right)\geq\zeta_n,\forall n. \tag{50c}$$

where ζ_n is the slack variable. The initial UAV trajectory is obtained until problem $\mathcal{P}_{\text{feasible}}^{\mathbf{q}}$ is successfully solved and $\zeta\geq 0,\ \forall n$.

C. Convergence and Complexity Analysis

1) Convergence Analysis: Proposition 1: The proposed Algorithm 1 provides a solution that converges to at least a locally optimal solution.

Proof: Let us define $\Pi(\boldsymbol{\tau}^j, \mathbf{q}^j)$ and $\Pi_{\rm lb}^{\mathbf{q}}(\boldsymbol{\tau}^j, \mathbf{q}^j)$ as the objective values of $\mathcal{P}_1^{\boldsymbol{\tau}}$ and $\mathcal{P}_{1.4}^{\mathbf{q}}$ at the j-th iteration. In the $(j+1)$-th iteration, at line 2 of Algorithm 1, we have

$$\Pi(\boldsymbol{\tau}^j, \mathbf{q}^j) \overset{\rm i}{\leq} \Pi(\boldsymbol{\tau}^{j+1}, \mathbf{q}^j). \tag{51}$$

The inequality (i) holds since $\boldsymbol{\tau}^{j+1}$ is an optimal solution of $\mathcal{P}_1^{\boldsymbol{\tau}}$. Then, at line 3 of Algorithm 1, we have

$$\begin{aligned}\Pi(\boldsymbol{\tau}^{j+1}, \mathbf{q}^j) &\overset{i2}{=} \Pi_{\rm lb}^{\mathbf{q}}(\boldsymbol{\tau}^{j+1}, \mathbf{q}^j)\\ &\overset{i3}{\leq} \Pi_{\rm lb}^{\mathbf{q}}(\boldsymbol{\tau}^{j+1}, \mathbf{q}^{j+1}) \overset{i4}{\leq} \Pi(\boldsymbol{\tau}^{j+1}, \mathbf{q}^{j+1}).\end{aligned} \tag{52}$$

The equality $(i2)$ holds since the first-order Taylor approximation as in (38), (39), (42), and (48) are tight at given point $\mathbf{q}^j$, and the inequality $(i3)$ holds since $\mathbf{q}^{j+1}$ is an optimal solution of $\mathcal{P}_{1.4}^{\mathbf{q}}$. Furthermore, the inequality $(i4)$ holds since the optimal value of $\mathcal{P}_{1.4}^{\mathbf{q}}$ is a lower bound of $\mathcal{P}_1^{\mathbf{q}}$ at given $\mathbf{q}^{j+1}$. From (52) and (51), we have $\Pi(\boldsymbol{\tau}^j, \mathbf{q}^j) \leq \Pi(\boldsymbol{\tau}^{j+1}, \mathbf{q}^{j+1})$ which proves that the objective value of $\mathcal{P}_1$ is non-decreasing over the iterations. Moreover, the objective value of $\mathcal{P}_1$ is restricted by an upper bound value due to the limited total traveling time T, transmit power P_s, UB transmit power P_u, and maximum value of $\eta_{\max}$. Thus, the convergence of Algorithm 1 is assured. ■

2) Complexity Analysis: We provide the complexity analysis for Algorithm 1. Since the problem $\mathcal{P}_1^{\boldsymbol{\tau}}$ can be solved by using the proposed closed-form expressions, thus the complexity is mainly relied on addressing $\mathcal{P}_1^{\mathbf{q}}$. Moreover, the problem $\mathcal{P}_1^{\mathbf{q}}$ includes logarithmic form, thus its complexity is $\mathcal{O}(L_1(3N)^{3.5})$, where $3N$ is the number of scalar variables and L_1 is the number of iterations to update UB trajectory [54]. Then, the overall complexity of Algorithm 1 is $\mathcal{O}(L_2 L_1 (3N)^{3.5})$ where L_2 is the number of iterations until convergence.

IV. Proposed IA-Based Algorithm for Solving $\mathcal{P}_1$

In order to solve $\mathcal{P}_1$, we firstly introduce slack variables z_1^n and z_2^n such that $(H^2 + \|\mathbf{q}_n - \mathbf{w}_s\|^2) \leq (z_1^n)^{2/\alpha}$ and $(H^2 + \|\mathbf{q}_n - \mathbf{w}_d\|^2) \leq (z_2^n)^{2/\alpha}$, respectively. Then, let us denote $\mathbf{z} \triangleq \{z_1^n, z_2^n, n \in \mathcal{N}\}$, by which the problem $\mathcal{P}_1$ is rewritten as:

$$\mathcal{P}_2: \max_{\mathbf{q},\boldsymbol{\tau},\mathbf{z}} B\sum_{n\in\mathcal{N}} \tau_n \delta_t \log_2\left(1 + \frac{\Theta\left(\eta_u^n \omega_0 P_s + \bar{P}_u z_1^n\right)}{z_1^n z_2^n}\right) \tag{53a}$$

s.t.

$$\left(H^2 + \|\mathbf{q}_n - \mathbf{w}_s\|^2\right) \leq (z_1^n)^{2/\alpha}, \tag{53b}$$

$$\left(H^2 + \|\mathbf{q}_n - \mathbf{w}_d\|^2\right) \leq (z_2^n)^{2/\alpha}, \tag{53c}$$

$$B\sum_{n\in\mathcal{N}} \tau_n \delta_t \log_2\left(1 + \frac{e^{-E}\omega_0 P_s^n}{z_1^n \sigma_u^2}\right) + \sigma S \geq B\sum_{n\in\mathcal{N}} \tau_n \delta_t \log_2\left(1 + \frac{\Theta\left(\eta_u^n \omega_0 P_s + \bar{P}_u z_1^n\right)}{z_1^n z_2^n}\right), \tag{53d}$$

$$B\sum_{n\in\mathcal{N}} \tau_n \delta_t \log_2\left(1 + \frac{\Theta\left(\eta_u^n \omega_0 P_s + \bar{P}_u z_1^n\right)}{z_1^n z_2^n}\right) \geq S, \tag{53e}$$

$$\sum_{i=1}^{n}\left(E_{\rm fly}^n(\mathbf{q}) + \tau_n \delta_t\left(P_b + P_u\right)\right) \leq \sum_{i=1}^{n} \frac{\mu(1-\tau_n)\delta_t \omega_0 P_{\rm WPT}}{z_1^n}, \tag{53f}$$

$$\|\mathbf{q}_{n+1} - \mathbf{q}_n\| \leq \delta_d = V_{\max}\delta_t, n = 0, \ldots, N-1, \tag{53g}$$

$$\mathbf{q}_0 = \mathbf{q}_{\rm I}, \mathbf{q}_N = \mathbf{q}_{\rm F}, \tag{53h}$$

$$0 \leq \tau_n \leq 1, n \in \mathcal{N}, \tag{53i}$$

By applying Lemmas 2 and 3, $\mathcal{P}_2$ can be rewritten as:

$$\mathcal{P}_{21}: \max_{\mathbf{q},\boldsymbol{\tau},\mathbf{z}} B\sum_{n\in\mathcal{N}} \tau_n \delta_t \log_2\left(1 + \frac{\Theta\left(\eta_u^n \omega_0 P_s + \bar{P}_u z_1^n\right)}{z_1^n z_2^n}\right) \tag{54a}$$

s.t.

$$(53b), (53c), (53g), (53h), (53i), \tag{54b}$$

$$B\sum_{n\in\mathcal{N}} \tau_n \delta_t \Theta_1 + \sigma S \geq B\sum_{n\in\mathcal{N}} \tau_n \delta_t \Theta_2, \tag{54c}$$

$$B\sum_{n\in\mathcal{N}} \tau_n \delta_t \Theta_2 \geq S, \tag{54d}$$

$$\sum_{i=1}^{n}\left(E_{\rm fly}^n(\mathbf{q}) + \tau_n \delta_t\left(P_b + P_u\right)\right) \leq \sum_{i=1}^{n} \mu(1-\tau_n)\delta_t \omega_0 P_{\rm WPT} \tilde{z}_1^n. \tag{54e}$$

The problem $\mathcal{P}_{21}$ is still non-convex due to the non-convexity of constraints (54c)–(54e). First, we introduce an equivalent $\tau_n\Theta_i \triangleq 0.25 \times [(\tau_n + \Theta_i)^2 - (\tau_n - \Theta_i)^2], i \in \{1, 2\}$ and $\tau_n \tilde{z}_1^n \triangleq 0.25 \times [(\tau_n + \tilde{z}_1^n)^2 - (\tau_n - \tilde{z}_1^n)^2]$. Then, by applying the first-order Taylor at (j+1)-th iteration, it yields:

$$\begin{aligned}&\tau_n\Theta_i \\ &\geq \frac{(\tau_n^j + \Theta_i^j)^2}{4} + \frac{(\tau_n^j + \Theta_i^j)}{2} \times (\tau_n - \tau_n^j + \Theta_i - \Theta_i^j)\\ &- \frac{(\tau_n^j - \Theta_i^j)^2}{4} - \frac{(\tau_n^j - \Theta_i^j)}{2} \times (\tau_n - \tau_n^j - \Theta_i + \Theta_i^j) \triangleq \widehat{\Theta}_i^n.\end{aligned} \tag{55}$$

$$\begin{aligned}&\tau_n \tilde{z}_1^n \\ &\geq \frac{(\tau_n^j + \tilde{z}_1^{n,j})^2}{4} + \frac{(\tau_n^j + \tilde{z}_1^{n,j})}{2} \times (\tau_n - \tau_n^j + \tilde{z}_1^n - \tilde{z}_1^{n,j})\end{aligned}$$

Algorithm 2: Proposed IA-Based Iterative Algorithm to Solve $\mathcal{P}_1$.

Initialization: Set $j := 0$ and generate an initial feasible point $\mathbf{q}^j$, $\boldsymbol{\tau}^j$, $\mathbf{z}^{\mathbf{j}}$, $\mathbf{y}^{\mathbf{j}}$.

1: **repeat**

2: Solve (57a) to obtain the optimal solution $\mathbf{q}^\star$, $\boldsymbol{\tau}^\star$, $\mathbf{z}^\star$, $\mathbf{y}^\star$.

3: Update $\mathbf{q}^{j+1} \triangleq \mathbf{q}^\star$, $\boldsymbol{\tau}^{j+1} \triangleq \boldsymbol{\tau}^\star$, $\mathbf{z}^{\mathbf{j+1}} \triangleq \mathbf{z}^\star$, $\mathbf{y}^{\mathbf{j+1}} \triangleq \mathbf{y}^\star$

4: **until** Convergence

$$-\frac{(\tau_n^j - \tilde{z}_1^{n,j})^2}{4} - \frac{(\tau_n^j - \tilde{z}_1^{n,j})}{2} \times (\tau_n - \tau_n^j - \tilde{z}_1^n + \tilde{z}_1^{n,j}) \triangleq \widehat{z}_1. \tag{56}$$

To overcome the non-convexity of $E_{\text{fly}}^n(\mathbf{q})$, we apply the same manipulation as in (44)–(46), (48). Consequently, the problem $\mathcal{P}_{21}$ can be re-written as:

$$\mathcal{P}_{22}: \max_{\mathbf{q},\boldsymbol{\tau},\mathbf{z},\mathbf{y}} B\sum_{n\in\mathcal{N}} \delta_t \widehat{\Theta}_2 \tag{57a}$$

s.t.

$$(53b), (53c), (53g), (53h), (53i), \tag{57b}$$

$$B\sum_{n\in\mathcal{N}} \delta_t \widehat{\Theta}_1 + \sigma S \geq B\sum_{n\in\mathcal{N}} \delta_t \widehat{\Theta}_2, \tag{57c}$$

$$B\sum_{n\in\mathcal{N}} \delta_t \widehat{\Theta}_2 \geq S, \tag{57d}$$

$$\sum_{i=1}^{n} \left(\bar{E}_{\text{fly}}^n(\mathbf{q}) + \tau_n \delta_t \left(P_b + P_u\right)\right)$$

$$\leq \sum_{i=1}^{n} \mu \delta_t \omega_0 P_{\text{WPT}} \left(\tilde{z}_1^n - \widehat{z}_1\right), \tag{57e}$$

$$\frac{\delta_n^4}{y_n^2} \leq (y_n^j)^2 + 2y_n^j \left(y_n - y_n^j\right) - 2\kappa_2 \left\|\mathbf{q}_{n+1}^j - \mathbf{q}_n^j\right\|^2$$

$$+ 4\kappa_2 \left(\mathbf{q}_{n+1}^j - \mathbf{q}_n^j\right)^T \left(\mathbf{q}_{n+1} - \mathbf{q}_n\right), \forall n. \tag{57f}$$

The problem $\mathcal{P}_{22}$ is convex and thus it can be solved using standard solvers [55]. Finally, the pseudo code to solve (22a) is summarized in Algorithm IV.

A. Convergence and Complexity Analysis

1) Convergence Analysis: We observe that the Algorithm 2 is based on IA method, whereas its convergence was proved in [56], [57]. To be self-contained, we introduce the following proposition.

Proposition 2: The proposed Algorithm 2 a solution that converges to at least a locally optimal solution of problem $\mathcal{P}_1$.

Proof: See [7, Appendix D]. ■

2) Complexity Analysis: We now provide the complexity analysis for Algorithm 2. Because problem (57a) is convex, various solvers applying the interior point (IP) method can be utilized to solve effectively [53]. Specifically, problem (57a) involves $8N + 6$ linear and quadratic constraints, and $11N + 2$ scalar real variables. As a result, the computational complexity required to solve (57a) in each iteration is $\mathcal{O}(8N+6)^{0.5}(11N+2)^3$ [58, Chapter 6]. Consequently, the total complexity of $\mathcal{O}(L_3(8N+6)^{0.5}(11N+2)^3)$, whereas L_3 is the number of iterations to obtain an optimal solution.

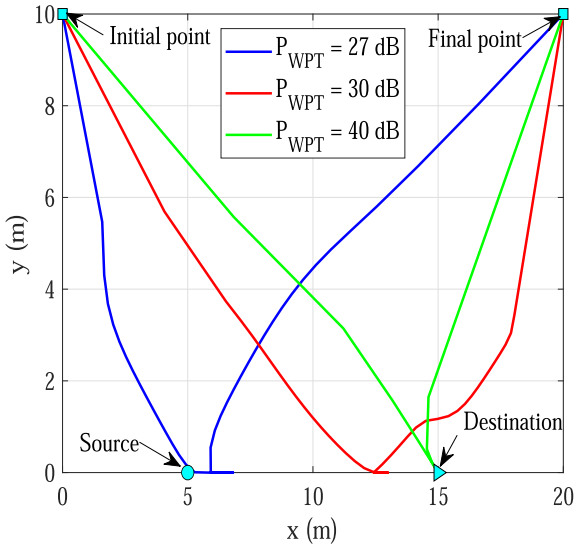

Fig. 2. UB trajectory with different values of P_{WPT}.

V. Simulation Results

In this section, the numerical results are given to validate the performance of our proposed scheme. We assume that the horizontal locations of the source and destination are set as $\mathbf{w}_s = [5m, 0]^T$ and $\mathbf{w}_s = [15m, 0]^T$, respectively. The UB's initial and final locations are respectively set $\mathbf{q}_{\text{I}} = [0, 10m]^T$ and $\mathbf{q}_{\text{F}} = [20m, 10m]^T$. The UB altitude is fixed at $H = 10$ meters with maximum transmit power $P_u \in [5, 10]$ mW and maximum velocity $V_{\max} = 20$ m/s [8]. Moreover, the transmit power of source S used for WPT and information transmission are set as $P_{\text{WPT}} \in [27, 40]$ dB [34] and $P_s = 16$ dBm, respectively. the power channel gain at reference distance $d = 1m$ is -30 dB [8] and the noise power at the source and destination is -90 dB [8]. The circuit power consumption of typical backscatter trasmitter is less than 1 μW [22], thus we set $P_b = 10^{-6}$ W. The maximum backscatter coefficient equals to 0.5 [49]. Each time slot duration equals to 0.5 s and energy harvesting coefficient is 0.84 [59], [60]. The system bandwidth is $B = 1$ Mhz. The error tolerance threshold of alternating algorithms is set to $\epsilon = 10^{-4}$. To highlight the designed algorithms, we compare our proposed methods with benchmark schemes. Specifically, benchmark schemes are described as follows:

- No caching (NC): Similar to Algorithm 1 but without caching capability.
- Fixed DTS ratio (FTau): Similar to Algorithm 1 but with fixed DTS ratio, $\tau_n = 0.5$.
- Fixed trajectory (LFTra): Similar to Algorithm 1 but with fixed trajectory, wherein the UB flies from initial position to the middle point between source and destination then it returns to the final position.

Fig. 2 illustrates the UB trajectories obtained for the proposed algorithm at different charging power values of the source, i.e., P_{WPT} equals to 27 dB, 30 dB, and 40 dB. Moreover, δ_t and $P_s =$

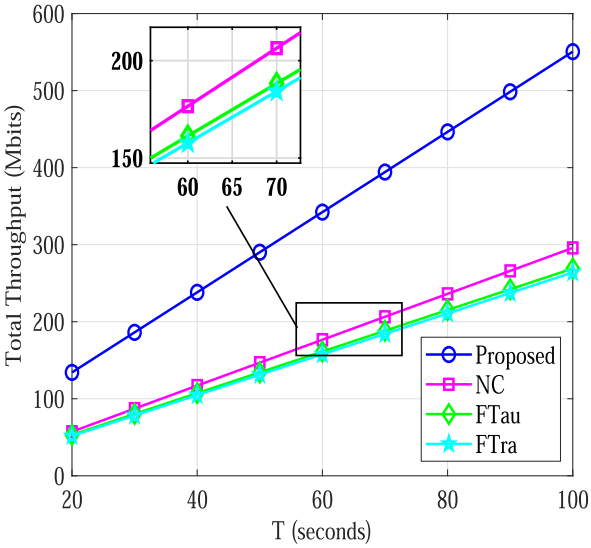

Fig. 3. Total throughput versus traveling time T.

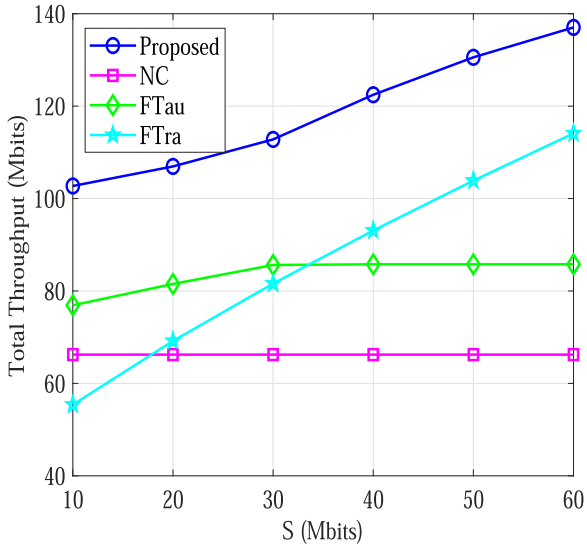

Fig. 4. Total throughput versus demanded data of the destination S.

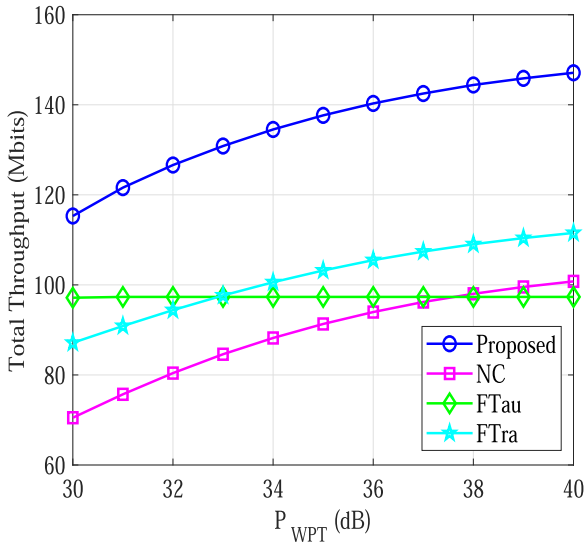

Fig. 5. Total throughput versus P_{WPT}.

are set as 0.5 s and 16 dBm, respectively. It can be seen from Fig. 2 that the P_{WPT} significantly affects the UB's trajectory. Specifically, the UB tends to fly from the initial point to the source node and then return back to the final location when P_{WPT} is equal to 27 dB. Besides, the UB can move towards the destination with the increase of P_{WPT} values. For instance, when the charging power of the source is increased from 27 dB to 40 dB, UB will move in the direction closer to the destination location to improve the total throughput. This is because when the P_{WPT} is small, the UB should fly closer to source S to improve the harvested energy, which can satisfy constraint (22a). Especially, the harvested energy is maximized as the UB can hover over the source location, as explained in the right-hand sight (RHS) of (22a). Furthermore, when the P_{WPT} value is high enough, the constraint (22a) can be guaranteed. Thus, the UB can fly closer to the destination to maximize achievable throughput.

In Fig. 3, we investigate the influence of total traveling time to the performance with $\delta_t = 0.5$ s, $P_s = 40$ mW, $P_u = 5$ mW, $S = 50$ Mbits, $P_{\mathrm{WPT}} = 33$ dB. We observe that all the algorithms are linearly increasing with a higher number of traveling time T (in seconds). This is expected since the total collected throughput at the destination is proportional to the reflection time as in (22a). As inferred from the results, the proposed algorithms significantly improve the total throughput (bps) as compared with the benchmarks. Specifically, at $T = 100$ seconds, the proposed algorithm can support a throughput up to 550.59 Mbps while the NC, FTau, FTra schemes respectively impose 295.85, 269.07, and 263.88. This demonstrates the superiority of our proposed method that jointly optimizes dynamic time splitting ratio and trajectory with caching at the UB compared to benchmark schemes with no caching capability, fixed DTS ratio, or fixed trajectory.

In Fig. 4, we study the influences of the demanded data S (in bits) to the total throughput, with $T = 30$ seconds, $P_s = 5$ mW, $V_{\max} = 20$ m/s, $H = 8$ m. We see that the performance of NC method is unaltered by increasing the demanded data S. This can be explained that since NC does not cache a part of requested file for data transmission to destination, we then have $\sigma S = 0$. Therefore, increasing the value of S has no effect on the NC scheme. Furthermore, our proposed algorithm performs much better than benchmark ones. Specifically, at $S = 60$ Mbits, the jointly optimization method can serve 137.03 Mbits while the NC, FTau, and FTra achieve less than 51.66%, 37.39%, and 16.71%, respectively. One more interesting point that can be observed from Fig. 4 is that the FTau scheme can achieve a better performance than FTra when the demanded data is small, i.e., $S < 30$ Mbits. Nevertheless, FTau's performance has deteriorated compared to FTra when $S > 30$ Mbits. Particularly, the performance of FTra is converged to a saturation value by growing S. This is because the total throughput is restricted by other resources, i.e., transmit power P_s, traveling time T, reflection time τ_n.

Fig. 5 illustrated the influences of the charging power of the source S on the achievable throughput of all schemes, with $P_u = 5$ mW, $P_s = 10$ mW, $\sigma = 0.7$, $T = 30$ seconds. First, we can see that the performance of the proposed, NC, and FTra is significantly enhanced with the increase of the P_{WPT} values while the NC performance looks unchanged. In fact, the

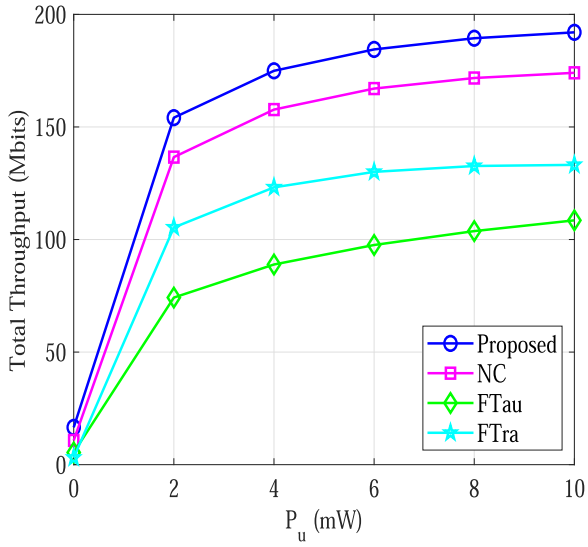

Fig. 6. Total throughput versus transmit power of the UAV P_u.

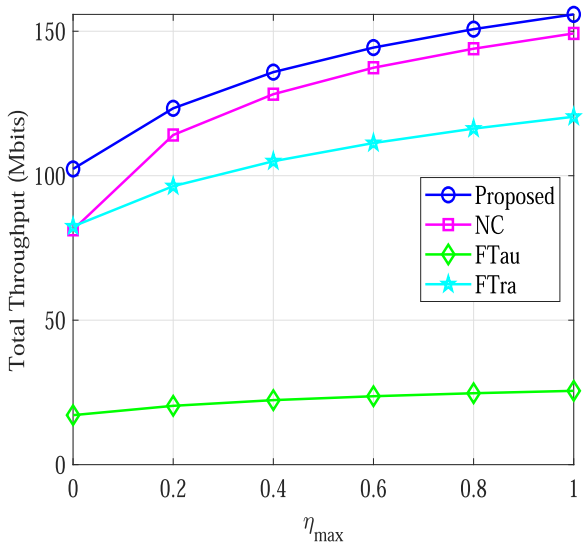

Fig. 7. Total throughput versus $\eta_{\max}$.

total throughput of the NC scheme is slightly increased from 97.15 to 97.33 Mbits when $P_{\rm WPT}$ is from 30 to 31 dB. This is because the more the transmit power is assigned, the higher the harvested energy is achieved. Therefore, the UB can have more reflection time, i.e., higher value of τ_n, which satisfies the energy constraints as in (10). Consequently, the system throughput is improved. However, because the NC scheme has a fixed τ value, the allocated time for data transmission is then unchanged, which restricts the NC's performance. Fig. 5 still shows the superiority of our proposed scheme over benchmark ones. More specifically, the Proposed, NC, FTAU, and FTra impose 115.3, 70.5, 97.15, and 87.14 Mbits when $P_{\rm WPT}$ equals 30 dB, respectively.

In Fig. 6, the total throughput is presented as a function of the transmit power of the UB P_u, where $T = 30$ seconds, $V_{\max} = 20$ m/s, $H = 5$ m, $S = 60$ Mbits. It is observed that the UB transmit power has dramatic impact on the total throughput obtained at the destination. Specifically, the obtained throughput of proposed scheme increases from 174.94 to 184.44 Mbits corresponding to P_u value equals to 4 and 6 mW, respectively. This is due to the fact that the total collected throughput depends on the transmit power P_u as shown in (22a). Specially, we also compare our schemes in the use case of both passive with active transmission and when we only use passive mode (i.e., $P_u = 0$). Obviously, all schemes' performance when used in the active and passive transmission is far superior to that when using only passive mode. Specifically, the total throughput of our proposed, NC, Ftau, and Ftra is 16.56, 10.76, 5.4, and 3.1 when $P_u = 0$, respectively, while it can respectively obtain 154.12, 136.6, 74.21, and 105.36 when $P_u = 2$ mW. Nevertheless, increasing P_u does not always significantly improve network performance. For example, the performance of the Proposed scheme only slightly increases from 189.41 to 192.03 when P_u from 8 to 10 mW. This is because the throughput depends not only on transmit power of UB, but also on other factors such as bandwidth, flying time, source transmit power.

Fig. 7 presents an evaluation of the total throughput versus the maximum value of backscatter coefficient $\eta_{\max}$, with $T = 100$ seconds, $V_{\max} = 20$ m/s, $H = 8$ m, $P_u = 5$ mW, $S = 50$ Mbits, and $T = 20$ seconds. It is observed that the achievable throughput of all schemes is dramatically improved with the increase of the backscattering coefficient $\eta_{\max}$. Specifically, at $\eta_{\max} = 0.2$ (or 0.4), the total throughput of the proposed scheme is 123.33 Mbits (or 135.85 Mbits), respectively, while the NC obtains less than 7.49% (or 5.62%). Whereas the FTau and FTra respectively impose less than 83.49% (or 83.56 %) and 21.85% (or 22.7%) compared to the proposed method. Particularly, we also depict the total throughput of all schemes in the case of no backscattering communications, i.e., $\eta_{\max} = 0$. Specifically, our proposed method is still better than other benchmarks in this scenario. Moreover, the performance of NC is worse than FTra, and the FTau is still the worst one. This demonstrates the superiority of our proposed joint optimization compared to other methods in practice with different parameters.

Figs. 8(a) and 8(b) depict the plot of the total throughput and total computational time as functions of the total traveling time (seconds), with $V_{\max} = 20$ m/s, $P_s = 20$ dB, $S = 150$ Mbits. It is shown from 8 a that the BCD-based algorithm slightly enhances the total throughput compared with the IA-based algorithm for all values of T. For instance, when the total traveling time is 80 and 100 seconds, the total throughput of the BCD is 526.9 and 655.62 Mbits, respectively. While the IA respectively imposes lower 1.8% and 1.38% compared to the BCD method one. We also observe from Fig. 8(b) that the total computational time of both proposed methods is significantly increased with a higher number of flying time T. For instance, when the UAV traveling time equals 50, 70, and 90, the computational time of the BCD method is 62.62, 107.3, and 177.64 seconds, respectively. Moreover, the computational time of the IA method is much higher than that as compared to BCD one. For example, when T is equal to 80 and 100 seconds, the running time of the IA-based algorithm is higher than the BCD-based algorithm by 42.12% and 36.23%, respectively. This is because the complexity of the BCD method mainly depends on trajectory optimization since we can obtain the closed-form expression for the optimal value of DTS. Therefore, the computational time of the BCD is significantly decreased. While using the IA method, we need to optimize all variables, i.e., $\mathbf{q}$, $\boldsymbol{\tau}$, $\mathbf{z}$, $\mathbf{y}$ of $\mathcal{P}_{22}$, in each iteration, which increases

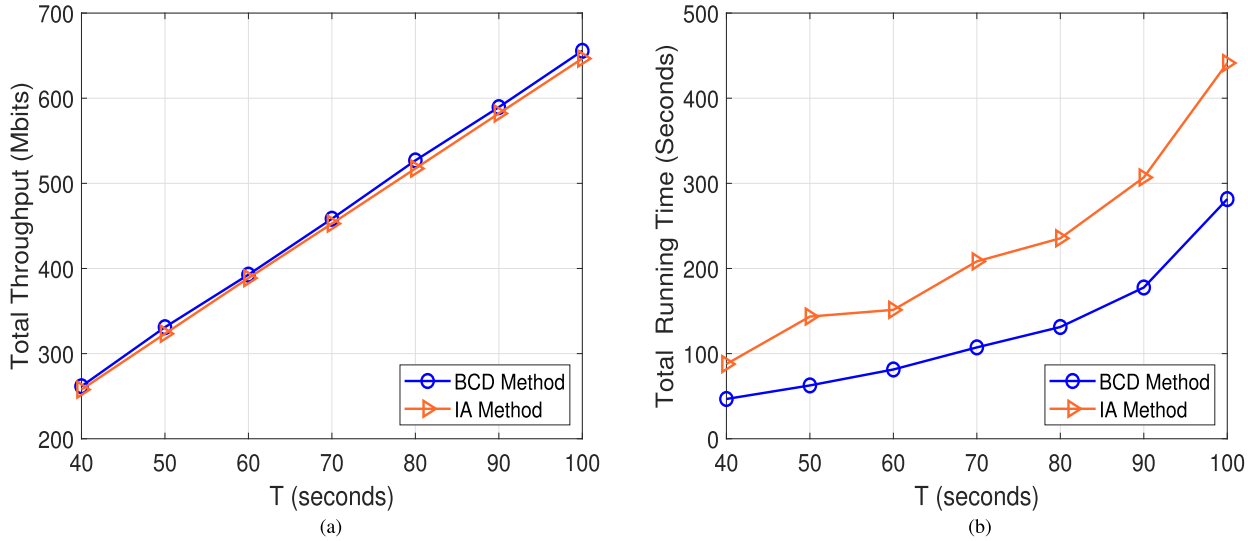

Fig. 8. Total throughput and running time vs. traveling time T. (a) Total Throughput. (b) Computational Time (Seconds).

the number of variables and quadratic constraints compared to the BCD method, i.e., as shown in Section IV: A-2. Inspired by interesting observations in Figs. 8(a) and 8(b), we can obtain a similar performance, i.e., total throughput, and greatly reduce the computational time while applying the BCD-based algorithm to solve our problem instead of using the IA-based algorithm.

VI. Conclusion and Future Directions

In this paper, a new self-energized EH model has been proposed to power the UAV communications. In this context, we have investigated the cache-assisted wireless powered UAV-enabled backscatter communciations. Specifically, we maximized the total throughput via jointly optimizing DTS ratio and trajectory. The formulated problem was non-convex which is troublesome to solve. Thus, we proposed efficient alternating algorithm based on BCD method and SCA technique to solve it. Particularly, the optimal DTS ratio for a given UB trajectory was derived in closed-form expression which significantly reduced the complexity of proposed solutions. We illustrated via simulation results that the proposed methods outperformed reference schemes in term of total throughput. Particularly, the simulation results showed the superiority of our design over scenarios with active or passive transmission only. In particular, the simulation results also show the advantages of the BCD-based method compared to the IA-based algorithm.

The outcome of this work will motivate future research directions: i. The study of a multi-antenna UAV system, which increases complexity but might further improve the system performance; ii. Another promising direction is to consider intelligent reflecting surface (IRS); iii. The study of a more general system model with multiple UAVs and multiple ground users.

Appendix A
Proof of Lemma 1

Proof for (20): Firstly, we consider a function $f(x) = \mathbb{E}_X[\log_2(1+e^{\ln x})]$, $x>0$. Based on Jensen's inequality for convex function $\log_2(1+e^{\ln x})$, we have

$$f(x) \geq \log_2\left(1+e^{\mathbb{E}_X[\ln x]}\right). \tag{A.1}$$

Let us denote $x \triangleq P_s|h_{su}^n|^2/\sigma_u^2$ and apply [61, 4.331.1], we then have

$$\begin{aligned}\mathbb{E}_X[\ln x] &= \int_0^{+\infty} \lambda_{su} e^{-\lambda_{su}x} \ln x dx = -(\ln \lambda_{su} + E)\\ &= \ln\left(P_s\omega_0 (d_{su}^n)^{-\alpha}/\sigma_u^2\right) - E,\end{aligned} \tag{A.2}$$

where E is the Euler-Mascheroni constant, i.e., $E = 0.5772156649$ as in [61, 8.367.1]; $\mathbb{E}[x] = P_s\omega_0(d_{su}^n)^{-\alpha}/\sigma_u^2$, and $\lambda_{su} = (\mathbb{E}[x])^{-1} = (P_s\omega_0(d_{su}^n)^{-\alpha}/\sigma_u^2)^{-1}$.

By substituting (A.2) into (A.1), we obtain the equation expression (20).

Proof for (21): Secondly, we consider a function $f(x,y) = \mathbb{E}_{X,Y}[\log_2(1+xy)]$, $x>0$, $y>0$, whereas x and y are two independent random variables. Based on Jensen's inequality for concave function $\log_2(1+xy)$ with respect to (w.r.t.) y, we have

$$f(x,y) \leq \mathbb{E}_X\left[\log_2\left(1+x\mathbb{E}_Y[y]\right)\right] \triangleq \hat{f}(x,y). \tag{A.3}$$

Then, by applying Jensen's inequality for convex function $\log_2(1+e^{\ln x})$ with respect to (w.r.t.) x, we have

$$\begin{aligned}\hat{f}(x,y) &= \mathbb{E}_X\left[\log_2\left(1+e^{\ln x}\mathbb{E}_Y[y]\right)\right]\\ &\geq \log_2\left(1+e^{\mathbb{E}_X[\ln x]}\mathbb{E}_Y[y]\right) \triangleq \tilde{f}(x,y).\end{aligned} \tag{A.4}$$

From (A.3) and (A.4), we see that $\tilde{f}(x,y)$ can serve as an approximation function of $f(x,y)$ but it is not a lower bound or an upper bound of $f(x,y)$.

Let us denote $x \triangleq |h_{ud}^n|^2$, $y \triangleq \frac{\eta_u^n P_s|h_{su}^n|^2+\bar{P}_u}{\sigma_d^2}$, and apply [61, 4.331.1], we then have

$$\mathbb{E}_X[\ln x] = \int_0^{+\infty} \lambda_{su} e^{-\lambda_{su}x} \ln x dx = -(\ln \lambda_{su} + E)$$

$$= \ln \frac{\omega_0}{\left(H^2 + \|\mathbf{q}_n - \mathbf{w}_d\|^2\right)^{\alpha/2}} - E, \quad \text{(A.5)}$$

$$\mathbb{E}_Y[y] = \mathbb{E}\left[\psi_{ud}|\tilde{h}^n_{ud}|^2\right] = \frac{\eta^n_u P_s \omega_0 (d^n_{su})^{-\alpha} + \bar{P}_u}{\sigma^2_d}, \quad \text{(A.6)}$$

where $\mathbb{E}[x] = \frac{\omega_0}{(H^2+\|\mathbf{q}_n-\mathbf{w}_d\|^2)^{\alpha/2}}$, and $\lambda_{su} = (\mathbb{E}[x])^{-1} = (\frac{\omega_0}{(H^2+\|\mathbf{q}_n-\mathbf{w}_d\|^2)^{\alpha/2}})^{-1}$. Substituting (A.5) and (A.6) into (A.4), we obtain (21). Thus, the Lemma 1 is proof.

Appendix B
Proof of Theorem 1

It is easy to verify that if $\lambda_4 \neq 0$, thus $J(\boldsymbol{\tau}) = 0$ implying that $\tau_n = 1$ which is not a feasible solution. Thus, we conclude that $\lambda_4 = 0$.

In order to obtain the feasible solution, we evaluate all the cases as follows:

Case I: $\lambda_1 = 0 \Rightarrow G(\boldsymbol{\tau}) \neq 0$, $\lambda_2 = 0 \Rightarrow H(\boldsymbol{\tau}) \neq 0$, $\lambda_3 = 0 \Rightarrow I(\boldsymbol{\tau}) \neq 0$.

From (30), we have $\sum_{n\in\mathcal{N}} \delta_t \bar{R}^n_d = 0$ which is unreasonable. Thus, this case can not occur.

Case II: $\lambda_1 = 0 \Rightarrow G(\boldsymbol{\tau}) \neq 0$, $\lambda_2 \neq 0 \Rightarrow H(\boldsymbol{\tau}) = 0$, $\lambda_3 = 0 \Rightarrow I(\boldsymbol{\tau}) \neq 0$.

From (30), we find that $\lambda_2 = -1$ which is unreasonable. Thus, this case can not occur.

Case III: $\lambda_1 \neq 0 \Rightarrow G(\boldsymbol{\tau}) = 0$, $\lambda_2 = 0 \Rightarrow H(\boldsymbol{\tau}) \neq 0$, $\lambda_3 = 0 \Rightarrow I(\boldsymbol{\tau}) \neq 0$.

From (30), we have $\lambda_1 = \frac{\sum_{n\in\mathcal{N}} \delta_t \bar{R}^n_d}{\sum_{n\in\mathcal{N}} \delta_t \bar{R}^n_d - \sum_{n\in\mathcal{N}} \delta_t \bar{R}^n_u}$. If $\bar{R}^n_u = \bar{R}^n_d$, then we obtain $\lambda_1 = +\infty$. If $\bar{R}^n_u > \bar{R}^n_d$, then we obtain $\lambda_1 < 0$. All of these scenarios is unreasonable. If $\bar{R}^n_u < \bar{R}^n_d$, then we obtain $\lambda_1 > 1$. Furthermore, from $G(\boldsymbol{\tau}) = 0$, we have

$$\tau^\star_n \triangleq \frac{\sigma S}{N\delta_t(\bar{R}^n_d - \bar{R}^n_u)}. \quad \text{(B.1)}$$

Based on (34), the optimal solution $\{\tau^\star_n\}$ can be obtained iff $\bar{R}^n_u < \bar{R}^n_d, \forall n \in \mathcal{N}$.

Case IV: $\lambda_1 = 0 \Rightarrow G(\boldsymbol{\tau}) \neq 0$, $\lambda_2 \neq 0 \Rightarrow H(\boldsymbol{\tau}) = 0$, $\lambda_3 \neq 0 \Rightarrow I(\boldsymbol{\tau}) = 0$.

From $H(\boldsymbol{\tau}) = 0$, we have $\tau_n = \frac{S}{N\delta_t \bar{R}^n_d}$. From $I(\boldsymbol{\tau}) = 0$, we obtain $\tau_n = \frac{\chi_1 - E^n_{\text{fly}}(\mathbf{q})}{\chi_1 + \delta_t(P_b + P_u)}$. It can be seen that there exists two different optimal values of τ which is contradictory. Hence, this case is not occur.

Case V: $\lambda_1 \neq 0 \Rightarrow G(\boldsymbol{\tau}) = 0$, $\lambda_2 = 0 \Rightarrow H(\boldsymbol{\tau}) \neq 0$, $\lambda_3 \neq 0 \Rightarrow I(\boldsymbol{\tau}) = 0$.

Case VI: $\lambda_1 \neq 0 \Rightarrow G(\boldsymbol{\tau}) = 0$, $\lambda_2 \neq 0 \Rightarrow H(\boldsymbol{\tau}) = 0$, $\lambda_3 = 0 \Rightarrow I(\boldsymbol{\tau}) \neq 0$.

Similar to case IV, we also obtain two different values of τ in case V and VI which is conflict. Thus, these cases are not occur.

Case VII: $\lambda_1 \neq 0 \Rightarrow G(\boldsymbol{\tau}) = 0$, $\lambda_2 \neq 0 \Rightarrow H(\boldsymbol{\tau}) = 0$, $\lambda_3 \neq 0 \Rightarrow I(\boldsymbol{\tau}) = 0$.

In this special scenario, we obtain up to three different values of τ which is unreasonable. Thus, this case is not occur.

Case VIII: $\lambda_1 = 0 \Rightarrow G(\boldsymbol{\tau}) \neq 0$, $\lambda_2 = 0 \Rightarrow H(\boldsymbol{\tau}) \neq 0$, $\lambda_3 \neq 0 \Rightarrow I(\boldsymbol{\tau}) = 0$.

From (30), we have

$$\sum_{n\in\mathcal{N}} \delta_t \bar{R}^n_d - \lambda_3 \left(\chi_1 + \sum_{n\in\mathcal{N}} \delta_t \left(P_b + P_u\right)\right) = 0$$

$$\iff \lambda_3 = \frac{\sum_{n\in\mathcal{N}} \delta_t \bar{R}^n_d}{\chi_1 + \sum_{n\in\mathcal{N}} \delta_t \left(P_b + P_u\right)}. \quad \text{(B.2)}$$

Moreover, from $I(\boldsymbol{\tau}) = 0$, we have

$$\tau^\star_n = \frac{\chi_1 - E^n_{\text{fly}}(\mathbf{q})}{\chi_1 + \delta_t \left(P_b + P_u\right)}. \quad \text{(B.3)}$$

From (B.1), (B.3), and constraint (23a), we can obtain (35) which completes the proof of Theorem 1.

Appendix C

First, we proof the convexity of function $f(x) = \log_2(1 + 1/x)$. By taking the second derivative of $f(x)$, we have

$$f''(x) = \frac{(1+2x)}{x^2(1+x)^2 \ln 2}. \quad \text{(C.1)}$$

It is easy to see that $f''(x) > 0$ with $x > 0$, thus function $f(x)$ is convex.

Second, we proof the convexity of function $f(x) = \log_2(1 + (A_2 + A_3 x)/xy)$. The Hessian matrix of $f(x)$ can be calculated as

$$\boldsymbol{H}_f = \begin{bmatrix} \frac{A_2(A_2+2x(A_3+y))}{x^2(A_2+x(A_3+y))^2 \ln 2} & \frac{A_2}{(A_2+x(A_3+y))^2 \ln 2} \\ \frac{A_2}{\left(A_2+x\left(A_3+y\right)\right)^2 \ln 2} & \frac{(A_2+A_3x)(A_2+x(A_3+2y))}{y^2(A_2+x(A_3+y))^2 \ln 2} \end{bmatrix} \quad \text{(C.2)}$$

Based on (C.2), it can be seen that all elements of matrix $\boldsymbol{H}_f$ is positive values, with $A_2, A_3, x, y > 0$. For ease of notation, we denote $\boldsymbol{H}_f \triangleq \begin{bmatrix} \vartheta_1 & \varsigma \\ \varsigma & \vartheta_2 \end{bmatrix}$, with $\vartheta_1 \triangleq \frac{A_2(A_2+2x(A_3+y))}{x^2(A_2+x(A_3+y))^2 \ln 2}$, $\varsigma \triangleq \frac{A_2}{(A_2+x(A_3+y))^2 \ln 2}$, $\vartheta_2 \triangleq \frac{(A_2+A_3x)(A_2+x(A_3+2y))}{y^2(A_2+x(A_3+y))^2 \ln 2}$. Then we have:

$$\begin{aligned} x^T \boldsymbol{H}_f x &= [x_1 \ x_2] \begin{bmatrix} \vartheta_1 & \varsigma \\ \varsigma & \vartheta_2 \end{bmatrix} \begin{bmatrix} x_1 \\ x_2 \end{bmatrix} \\ &= [x_1\vartheta_1 + \varsigma x_2 \quad x_1\varsigma + x_2\,\vartheta_2] \begin{bmatrix} x_1 \\ x_2 \end{bmatrix} \\ &= (x_1)^2\vartheta_1 + \varsigma(x_2)^2 + (x_1)^2\varsigma + (x_2)^2\vartheta_2 \geq 0, \\ &\quad \forall x_1, x_2 \in \mathbb{R}^2 \backslash \{0\}. \end{aligned} \quad \text{(C.3)}$$

From (C.3), we can conclude that function $f(x)$ is convex since the Hessian matrix $\boldsymbol{H}_f$ is positive semi-definite [55].

References

[1] M. Mozaffari, W. Saad, M. Bennis, Y. Nam, and M. Debbah, "A tutorial on UAVs for wireless networks: Applications, challenges, and open problems," *IEEE Commun. Surv. Tut.*, vol. 21, no. 3, pp. 2334–2360, Jul.–Sep. 2019.

[2] Y. Zeng, Q. Wu, and R. Zhang, "Accessing from the sky: A tutorial on UAV communications for 5G and beyond," *Proc. IEEE*, vol. 107, no. 12, pp. 2327–2375, Dec. 2019.

[3] D.-H. Tran, T. X. Vu, S. Chatzinotas, S. ShahbazPanahi, and B. Ottersten, "Coarse trajectory design for energy minimization in UAV-enabled," *IEEE Trans. Veh. Technol.*, vol. 69, no. 9, pp. 9483–9496, Sep. 2020.

[4] H. Tran-Dinh, T. X. Vu, S. Chatzinotas, and B. Ottersten, "Energy-efficient trajectory design for UAV-enabled wireless communications with latency constraints," in *Proc. 53rd Asilomar Conf. Signals, Syst., Comput.*, 2019, pp. 347–352.

[5] Y. Zeng, J. Xu, and R. Zhang, "Energy minimization for wireless communication with rotary-wing UAV," *IEEE Trans. Wireless Commun.*, vol. 18, no. 4, pp. 2329–2345, Apr. 2019.

[6] M. Mozaffari, W. Saad, M. Bennis, and M. Debbah, "Mobile unmanned aerial vehicles (UAVs) for energy-efficient Internet of Things communications," *IEEE Trans. Wireless Commun.*, vol. 16, no. 11, pp. 7574–7589, Dec. 2017.

[7] D.-H. Tran, V.-D. Nguyen, S. Chatzinotas, T. X. Vu, and B. Ottersten, "UAV relay-assisted emergency communications in IoT networks: Resource allocation and trajectory optimization," *IEEE Trans. Wireless Commun.*, vol. 21, no. 3, pp. 1621–1637, Mar. 2021.

[8] M. Hua, L. Yang, C. Li, Q. Wu, and A. L. Swindlehurst, "Throughput maximization for UAV-aided backscatter communication networks," *IEEE Trans. Commun.*, vol. 68, no. 2, pp. 1254–1270, Feb. 2020.

[9] J. Stewart, "Google tests drone deliveries in project wing trials," BBC, Aug. 2014. [Online] Available: https://www.bbc.com/news/technology-28964260

[10] L. Kelion, "Facebook's laser drones vs Google's net-beaming balloons," *BBC News*, 2015. [Online]. Available: http://www.bbc.com/news/technology-34780127

[11] Qualcom, "Paving the path to 5G: Optimizing commercial LTE networks for drone communication," Oct. 2018. [Online]. Available: https://www.qualcomm.com/news/onq/2016/09/06/paving-path-5goptimizing-commercial-lte-networks-drone-communication

[12] X. Zhong, Y. Guo, N. Li, and Y. Chen, "Joint optimization of relay deployment, channel allocation, and relay assignment for UAVs-Aided D2D networks," *IEEE/ACM Trans. Netw.*, vol. 28, no. 2, pp. 804–817, Apr. 2020.

[13] L. Li, T. Chang, and S. Cai, "UAV positioning and power control for two-way wireless Relaying," *IEEE Trans. Wireless Commun.*, vol. 19, no. 2, pp. 1008–1024, Feb. 2020.

[14] P. K. Sharma and D. I. Kim, "Secure 3D mobile UAV relaying for hybrid satellite-terrestrial networks," *IEEE Trans. Wireless Commun.*, vol. 19, no. 4, pp. 2770–2784, Apr. 2020.

[15] X. Sun, W. Yang, Y. Cai, Z. Xiang, and X. Tang, "Secure transmissions in millimeter wave SWIPT UAV-based relay networks," *IEEE Wireless Commun. Lett.*, vol. 8, no. 3, pp. 785–788, Jun. 2019.

[16] D. H. Tran, C. Symeon, and O. Bjorn, "Satellite- and cache-assisted UAV: A joint cache placement, resource allocation, and trajectory optimization for 6G aerial networks," *IEEE Open J. Veh. Technol.*, vol. 3, pp. 40–54, 2022, doi: 10.1109/OJVT.2022.3142170.

[17] H. Ye, X. Kang, J. Joung, and Y. Liang, "Optimization for full-duplex rotary-wing UAV-enabled wireless-powered IoT networks," *IEEE Trans. Wireless Commun.*, vol. 19, no. 7, pp. 5057–5072, Jul. 2020.

[18] G. Yang, R. Dai, and Y.-C. Liang, "Energy-efficient UAV backscatter communication with joint trajectory design and resource optimization," in *IEEE Trans. Wireless Commun.*, vol. 20, no. 2, pp. 926–941, Feb. 2021, doi: 10.1109/TWC.2020.3029225.

[19] A. Farajzadeh, O. Ercetin, and H. Yanikomeroglu, "UAV data collection over NOMA backscatter networks: UAV altitude and trajectory optimization," in *Proc. IEEE Intern. Conf. Commun.*, 2019, pp. 1–7.

[20] A. Farajzadeh, O. Ercetin, and H. Yanikomeroglu, "Mobility-assisted over-the-air computation for backscatter sensor networks," *IEEE Wireless Commun. Lett.*, vol. 9, no. 5, pp. 675–678, May 2020.

[21] J. Hu, X. Cai, and K. Yang, "Joint trajectory and scheduling design for UAV aided secure backscatter communications," *IEEE Wireless Commun. Lett.*, vol. 9, no. 12, pp. 2168–2172, Dec. 2020.

[22] X. Lu, D. Niyato, H. Jiang, D. I. Kim, Y. Xiao, and Z. Han, "Ambient backscatter assisted wireless powered communications," *IEEE Wireless Commun.*, vol. 25, no. 2, pp. 170–177, Apr. 2018.

[23] P. X. Nguyen *et al.*, "Backscatter-assisted data offloading in OFDMA-Based wireless-powered mobile edge computing for IoT networks," *IEEE Internet Things J.*, vol. 8, no. 11, pp. 9233–9243, Jun. 2021.

[24] N. Van Huynh, D. T. Hoang, X. Lu, D. Niyato, P. Wang, and D. I. Kim, "Ambient backscatter communications: A contemporary survey," *IEEE Commun. Surv. Tut.*, vol. 20, no. 4, pp. 2889–2922, Oct.–Dec. 2018.

[25] Y. Zeng and R. Zhang, "Energy-efficient UAV communication with trajectory optimization," *IEEE Trans. Wireless Commun.*, vol. 16, no. 6, pp. 3747–3760, Jun. 2017.

[26] Y. Cai, Z. Wei, R. Li, D. W. K. Ng, and J. Yuan, "Joint trajectory and resource allocation design for energy-efficient secure UAV communication systems," *IEEE Trans. Commun.*, vol. 68, no. 7, pp. 4536–4553, Jul. 2020.

[27] T. D. Hieu *et al.*, "Stability-aware geographic routing in energy harvesting wireless sensor networks," *Sensors*, vol. 16, no. 5, 2016, Art. no. 696.

[28] Y. Sun, D. Xu, D. W. K. Ng, L. Dai, and R. Schober, "Optimal 3D-Trajectory design and resource allocation for solar-powered UAV communication systems," *IEEE Trans. Commun.*, vol. 67, no. 6, pp. 4281–4298, Jun. 2019.

[29] T. N. Nguyen *et al.*, "Throughput enhancement in FD-and SWIPT-enabled IoT networks over non-identical Rayleigh fading channels," *IEEE Internet Things J.*, to be published, doi: 10.1109/JIOT.2021.3120766.

[30] I. Krikidis, S. Timotheou, S. Nikolaou, G. Zheng, D. W. K. Ng, and R. Schober, "Simultaneous wireless information and power transfer in modern communication systems," *IEEE Commun. Mag.*, vol. 52, no. 11, pp. 104–110, Nov. 2014.

[31] P. T. Tin, T. N. Nguyen, D.-H. Tran, M. Voznak, V.-D. Phan, and S. Chatzinotas, "Performance enhancement for full-duplex relaying with time-switching-based SWIPT in wireless sensors networks," *Sensors*, vol. 21, no. 11, 2021, Art. no. 3847.

[32] E. Limer, "This drone could fly forever with wireless power," 2016. [Online]. Available: https://www.popularmechanics.com/flight/drones/a23023/wirelesspower-drone/

[33] GET, "Wirelessly powered drone," 2016. [Online]. Available: http://getcorp.com/wirelessly-powered-drone/

[34] S. Yin, L. Li, and F. R. Yu, "Resource allocation and basestation placement in downlink cellular networks assisted by multiple wireless powered UAVs," *IEEE Trans. Veh. Technol.*, vol. 69, no. 2, pp. 2171–2184, Feb. 2020.

[35] D. N. K. Jayakody, T. D. P. Perera, A. Ghrayeb, and M. O. Hasna, "Self-energized UAV-assisted scheme for cooperative wireless relay networks," *IEEE Trans. Veh. Technol.*, vol. 69, no. 1, pp. 578–592, Jan. 2020.

[36] H. Yan, Y. Chen, and S.-H. Yang, "UAV-Enabled wireless power transfer with base station charging and UAV power consumption," *IEEE Trans. Veh. Technol.*, vol. 69, no. 11, pp. 12883–12896, Nov. 2020.

[37] J. Erman, A. Gerber, M. Hajiaghayi, D. Pei, S. Sen, and O. Spatscheck, "To cache or not to cache: The 3G case," *IEEE Internet Comput.*, vol. 15, no. 2, pp. 27–34, Mar./Apr. 2011.

[38] S. Mehrizi, S. Chatterjee, S. Chatzinotas, and B. Ottersten, "Online spatiotemporal popularity learning via variational bayes for cooperative caching," *IEEE Trans. Commun.*, vol. 68, no. 11, pp. 7068–7082, Nov. 2020.

[39] X. Xu, Y. Zeng, Y. L. Guan, and R. Zhang, "Overcoming endurance issue: UAV-enabled communications with proactive caching," *IEEE J. Sel. Areas Commun.*, vol. 36, no. 6, pp. 1231–1244, Jun. 2018.

[40] F. Cheng, G. Gui, N. Zhao, Y. Chen, J. Tang, and H. Sari, "UAV-relaying-assisted secure transmission with caching," *IEEE Trans. Commun.*, vol. 67, no. 5, pp. 3140–3153, May 2019.

[41] M. Chen, M. Mozaffari, W. Saad, C. Yin, M. Debbah, and C. S. Hong, "Caching in the sky: Proactive deployment of cache-enabled unmanned aerial vehicles for optimized quality-of-experience," *IEEE J. Sel. Areas Commun.*, vol. 35, no. 5, pp. 1046–1061, May 2017.

[42] S. Chai and V. K. N. Lau, "Online trajectory and radio resource optimization of cache-enabled UAV wireless networks with content and energy recharging," *IEEE Trans. Signal Process.*, vol. 68, pp. 1286–1299, 2020.

[43] H. Wu, F. Lyu, C. Zhou, J. Chen, L. Wang, and X. Shen, "Optimal UAV caching and trajectory in aerial-assisted vehicular networks: A learning-based approach," *IEEE J. Sel. Areas Commun.*, vol. 38, no. 12, pp. 2783–2797, Dec. 2020.

[44] Y. Hu, M. Chen, W. Saad, H. V. Poor, and S. Cui, "Distributed multi-agent meta learning for trajectory design in wireless drone networks," *IEEE J. Sel. Areas Commun.*, vol. 39, no. 10, pp. 3177–3192, Oct. 2021.

[45] D.-H. Tran, S. Chatzinotas, and B. Ottersten, "Satellite- and cache-assisted UAV: A joint cache placement, resource allocation, and trajectory optimization for 6G aerial networks," *IEEE Open J. Veh. Technol.*, vol. 3, pp. 40–54, 2022.

[46] M. Giordani and M. Zorzi, "Non-terrestrial communication in the 6G era: Challenges and opportunities," *IEEE Netw.*, vol. 35, no. 2, pp. 244–251, Mar./Apr. 2021, doi: 10.1109/MNET.011.2000493.

[47] Y. Yuan, L. Lei, T. X. Vu, S. Chatzinotas, S. Sun, and B. Ottersten, "Energy minimization in UAV-aided networks: Actor-critic learning for constrained scheduling optimization," *IEEE Trans. Veh. Technol.*, vol. 70, no. 5, pp. 5028–5042, May 2021.

[48] B. Lyu, C. You, Z. Yang, and G. Gui, "The optimal control policy for RF-powered backscatter communication networks," *IEEE Trans. Veh. Technol.*, vol. 67, no. 3, pp. 2804–2808, Mar. 2017.

[49] S. Xiao, H. Guo, and Y.-C. Liang, "Resource allocation for full-duplex-enabled cognitive backscatter networks," *IEEE Trans. Wireless Commun.*, vol. 18, no. 6, pp. 3222–3235, Jun. 2019.
[50] X. Kang, Y.-C. Liang, and J. Yang, "Riding on the primary: A new spectrum sharing paradigm for wireless-powered IoT devices," *IEEE Trans. Wireless Commun.*, vol. 17, no. 9, pp. 6335–6347, Sep. 2018.
[51] S. Gong, X. Huang, J. Xu, W. Liu, P. Wang, and D. Niyato, "Backscatter relay communications powered by wireless energy beamforming," *IEEE Trans. Commun.*, vol. 66, no. 7, pp. 3187–3200, Jul. 2018.
[52] M. Hong, M. Razaviyayn, Z.-Q. Luo, and J.-S. Pang, "A unified algorithmic framework for block-structured optimization involving Big Data: With applications in machine learning and signal processing," *IEEE Signal Process. Mag.*, vol. 33, no. 1, pp. 57–77, Jan. 2016.
[53] S. Boyd and L. Vandenberghe, *Convex Optimization*. Cambridge, U.K.: Cambridge Univ. Press, 2004.
[54] G. Zhang, Q. Wu, M. Cui, and R. Zhang, "Securing UAV communications via joint trajectory and power control," *IEEE Trans. Wireless Commun.*, vol. 18, no. 2, pp. 1376–1389, Feb. 2019.
[55] S. Boyd, "Advances in convex optimization: Interior-point methods, cone programming, and applications," in *Proc. 41st IEEE Conf. Decis. Control*, vol. 4, 2002.
[56] B. Marks, "A general inner approximation algorithm for nonconvex mathematical programs," *Oper. Res.*, vol. 26, no. 4, pp. 681–683, 1978.
[57] A. Beck, A. Ben-Tal, and L. Tetruashvili, "A sequential parametric convex approximation method with applications to nonconvex truss topology design problems," *J. Glob. Optim.*, vol. 47, no. 1, pp. 29–51, May 2010.
[58] A. Ben-Tal and A. Nemirovski, *Lectures on Modern Convex Optimization: Analysis, Algorithms, and Engineering Applications*. Philadelphia, PA, USA: SIAM, 2001.
[59] N. Singh *et al.*, "A dual polarized multiband rectenna for RF energy harvesting," *AEU-Int. J. Electron. C.*, vol. 93, pp. 123–131, 2018.
[60] T. D. Hieu *et al.*, "Performance evaluation of relay selection schemes in beacon-assisted dual-hop cognitive radio wireless sensor networks under impact of hardware noises," *Sensors*, vol. 18, no. 6, 2018, Art. no. 1843.
[61] I. S. Gradshteyn and I. M. Ryzhik, *Table of Integrals, Series, and Products*. New York, NY, USA: Academic, 2014.

Dinh-Hieu Tran (Graduate Student Member, IEEE) was born in 1989, in Vietnam, growing up in Gia Lai. He received the B.E. degree from the Department Electronics and Telecommunication Engineering, Ho Chi Minh City University of Technology, Ho Chi Minh City, Vietnam, in 2012, the M.S. degree (with Hons.) in electronics and computer engineering from Hongik University, Seoul, South Korea, in 2017, and the Ph.D. degree in telecommunications engineering from the Signal Processing and Satellite Communications Group, University of Luxembourg, Esch-sur-Alzette, Luxembourg, in December 2021, under the supervision of Prof. Symeon Chatzinotas and Prof. Björn Ottersten. His research interests include non-terrestrial networks (UAVs and satellite), IoTs, mobile edge computing, caching, backscatter, and B5G for wireless communication networks. In 2016, he was the recipient of the Hongik Rector Award for his excellence during his master's study at Hongik University. He was the co-recipient of the IS3C 2016 Best Paper Award. In 2021, he was nominated for the Best Ph.D. Thesis Award at the University of Luxembourg.

Symeon Chatzinotas (Senior Member, IEEE) is currently a Full Professor and the Chief Scientist I of satellite communications and the Head of the Signal Processing and Satellite Communications Research Group, SnT, University of Luxembourg, Luxembourg. He coordinates research activities in communications and networking, acting as a PI in more than 20 projects and is the main representative for 3GPP, ETSI, and DVB. In the past, he was a Visiting Professor with the University of Parma, Parma, Italy, lecturing on 5G wireless networks. He was involved in numerous R&D projects for NCSR Demokritos, CERTH Hellas and CCSR, University of Surrey, Guildford, U.K. He has coauthored more than 450 technical papers in refereed international journals, conferences and scientific books. He was the co-recipient of the 2014 IEEE Distinguished Contributions to Satellite Communications Award and best paper awards at EURASIP JWCN, CROWNCOM, and ICSSC. He is currently on the Editorial Board of IEEE TRANSACTIONS ON COMMUNICATIONS, IEEE OPEN JOURNAL OF VEHICULAR TECHNOLOGY, and *International Journal of Satellite Communications and Networking*.

Björn Ottersten (Fellow, IEEE) was born in Stockholm, Sweden, in 1961. He received the M.S. degree in electrical engineering and applied physics from Linköping University, Linköping, Sweden, in 1986, and the Ph.D. degree in electrical engineering from Stanford University, Stanford, CA, USA, in 1990. He has held research positions with the Department of Electrical Engineering, Linköping University, Information Systems Laboratory, Stanford University, Katholieke Universiteit Leuven, Leuven, Belgium, and University of Luxembourg, Luxembourg. From 1996 to 1997, he was the Director of Research with ArrayComm, Inc., a start-up in San Jose, CA, USA, based on his patented technology. In 1991, he was appointed as a Professor of signal processing with the Royal Institute of Technology (KTH), Stockholm, Sweden. He was the Head of the Department for Signals, Sensors, and Systems, KTH, and Dean of the School of Electrical Engineering, KTH. He is currently the Director of the Interdisciplinary Centre for Security, Reliability and Trust, University of Luxembourg. He was the recipient of the IEEE Signal Processing Society Technical Achievement Award and been twice awarded the European Research Council advanced research grant. He has coauthored journal papers which was the recipient of the IEEE Signal Processing Society Best Paper Award in 1993, 2001, 2006, 2013, and 2019, and eight IEEE conference papers best paper awards. He has been the Board Member of IEEE Signal Processing Society and Swedish Research Council, and is also on the Boards of the EURASIP and Swedish Foundation for Strategic Research. He was an Associate Editor for IEEE TRANSACTIONS ON SIGNAL PROCESSING and the Editorial Board of the *IEEE Signal Processing Magazine*. He is currently a Member of the Editorial Boards of the IEEE OPEN JOURNAL OF SIGNAL PROCESSING, *EURASIP Signal Processing Journal*, *EURASIP Journal of Advanced Signal Processing* and *Foundations and Trends of Signal Processing*. He is a Fellow of EURASIP.